



PEOPLE'S DEMOCRATIC REPUBLIC OF ALGERIA
MINISTRY OF HIGHER EDUCATION AND



SCIENTIFIC RESEARCH

UNIVERSITY OF AKLI MOHAN OULHADJ

FACULTY OF SCIENCE AND APPLIED SCIENCE

Thesis submitted to obtain the Degree of Master

Domain: Mater Science.

Speciality: Material science.

Elaboration and Characterization of Indium Samarium Oxide
(ISO) Semiconductor Thin Film Using Pneumatic Spray
Pyrolysis.

Presented by:
OULDAMER Roza

Publicly defended on: 04/10/2021

In front of the Jury committee composed of:

BENAMARA Salem	MCB	UAMOB	president
ADDALA Samia	MCA	UAMOB	Supervisor
BOUHDJER Lazhar	MCA	UAMOB	Co-supervisor
ZITOUNE Hachemi	MAA	UAMOB	Examiner
RAHLI Amel	MAA	UAMOB	Examiner

Academic year 2020/2021

Acknowledgements

First and foremost, I would like to thank Allah Almighty for giving me the strength, knowledge, ability and opportunity to undertake this research study and to persevere and complete it satisfactorily. Whithout his blessings, this achievement would not have been possible.

From the bottom of my heart, I want to thank my parents for their guidance, support and encouragement, for bieng there for me, never leaving me and always loving me.

*I would like to express my deep and sincere gratitude to my supervisor, **Dr. S.Addala** and co-supervisor **Dr.L.Bouhdjer**. they have been there providing thier heartfelt support and guidance at all the times and have invaluable inspiration and suggestions in quest for knowledge. Without their insightful guidance and persistent help, this thesis would never have been accomplished.*

*My most grateful thank to **Mr.S.Benamara** for the honor that makes to me by accepting the presidency of this jury.*

*I take immense pleasure in thanking to **Mr.H.Zitoune** who agreed to accept to belong to the jury and to examine my work,*

*It is also very pleasant to thank, **Mrs.A.Rahli** for honoring me for being an examiner of this work,*

Rozaouldamer



Dedication

I will dedicate this modest work to

My father, My mother

who sacrificed for me, for their support, encouragement, love, and dedication to my success in my studies and my life; a million words would be too short.


My brothers and my sisters

for being there when I needed them, picking me up when I fell, for being my best friends that I have ever known.

All my cousins

All my family

All my friends



Contents

Acknowledgements

Dedication

Contents **I**

List of figures **IV**

List of tables **V**

Abreviation **VI**

General introduction **1**

Chapter I : General concept

I.1 Introduction **3**

I.2 Thin films **3**

I.2.1 Definition **3**

I.2.2 Steps of the formation and the growth of thin-film using chemical vapor deposition technique **4**

a) Nucleation **4**

b) Coalescence step **6**

c) Growth step **6**

I.2.3 Thin film growth mode **7**

I.2.3.1 Layer type (called Frank and Van Der Merwe) **7**

I.2.3.2 Islands type (called Volmer-Weber) **7**

I.2.3.3 Mixed type (called Stransky-krastanov) **8**

I.3 Transparent conducting oxides **8**

I.3.1 Definition **9**

I.3.2 TCOs properties **9**

I.3.2.1 Electrical properties **9**

I.3.2.2 Optical properties **11**

I.3.3 Criteria for choosing TCO **14**

I.3.4 Application of TCO **14**

I.4 Indium oxide	15
I.4.1 Structural properties	15
I.4.2 Electrical properties	18
I.4.3 Optical properties	19
I.4.4 Application of In ₂ O ₃	20
I.5 Rare-earth	22
I.5.1 Generality	22
I.5.2 Common properties of the rare-earth	23
I.5.3 Atomic structure	24
I.5.4 Samarium chloride	24
Conclusion	25

Chapter II: Thin films: Elaboration techniques

II.1 Introduction	26
Section 1: Elaboration techniques	
II.2 Physical deposition processes	27
II.2.1 Sputtering	27
II.2.2 Molecular Beam Epitaxy (MBE)	29
II.2.3 Pulsed laser deposition	30
II.3 Chemical Deposition process	30
II.3.1 Sol-Gel	31
a) Dip-coating (SGDC)	32
b) Spin-coating	33
II.3.2 Spray pyrolysis	34
II.3.3 Chemical Vapor Deposition(CVD)	35
Section 2: Experimental procedure (protocol)	
II.4 Choosing the technique	36
II.5 Pneumatic spray pyrolysis technique	36
II.5.1 Working principle	36
II.5.2 Atomizer modes	37
II.5.3 Processing steps of pneumatic spray pyrolysis technique	37

II.5.3.1 Atomization of precursor solution	38
II.5.3.2 Aerosol transport	38
II.5.3.3 Precursor decomposition	38
II.5.4 Advantages of spray pyrolysis technique	39
II.6 Experimental procedure	40
II.6.1 Used montage	40
II.6.2 The choice of the substrate	41
II.6.3 Preparation of the substrate	42
II.6.4 Preparation of the solution (precursor)	44
II.6.5 Experimental conditions	45
II.6.6 Deposition process	46

Chapter III: Characterization, Results and Discussion

III.1 Characterization methods	47
III.1.1 X-rays diffractometer (XRD)	47
a) X-ray diffractometer principal	47
b) Information obtained from the X-ray Diffractogram	49
III.1.2 Scanning electron microscopy (SEM)	50
III.1.3 UV-Visible spectroscopy	51
III.2 Results and discussion	53
III.2.1 Structural study	53
a) Lattice parameters	55
b) Crystallites size	55
III.2.2 Surface and morphological study	55
III.2.3 Optical study	57
Conclusion	60

General conclusion	61
Bibliographic references	62
Abstract	

List of Figures

Figures of Chapter I

Figure I. 1: Schematic of thin-film deposited onto a substrate.	3
Figure I. 2: Adsorption, desorption and the nucleation process.	5
Figure I. 3: representation of thin- films nucleation:	5
Figure I. 4: The process of coalescence.	6
Figure I. 5: The process of growth and formation of the thin film.	7
Figure I. 6: Illustration of the different modes.	8
Figure I. 7: Schematic representation of processes leading to nucleation and 3-D (upper right) and 2-D (lower right) film growth.	8
Figure I. 8: Diagram of the optical widening effect of the Moss-Burstein shift.	12
Figure I. 9: Transmission spectrum of TCOs.	13
Figure I. 10: some applications of TCO.	15
Figure I. 11: In_2O_3 bixbyte cubic structure.	16
Figure I. 12: The coordination arrangement of In atoms.	16
FigureI. 13: Schematic representation of the sites In(1) in the bixbyite structure of In_2O_3 .	17
Figure I. 14: Schematic representation of the sites In(2) in the bixbyite structure of In_2O_3 .	17
Figure I. 15: Rhombohedral polymorph structure of In_2O_3 .	18
Figure I. 16: Electronic band structure of In_2O_3 .	19
Figure I. 17: Optical absorption of In_2O_3 at ≈ 3.7 eV.	20
Figure I. 18: Schematic of chemical gas sensor.	21
Figure I. 19: Rare earth element (red box) in mendeleev periodic table.	23
Figure I. 20: Samarium (III) chloride hexahydrate.	24
Figure I. 21: Crystal structure of SmCl_3 .	24

Figures of Chapter II

Figure II. 1: The classification of thin film deposition methods.	26
Figure II. 2: Basic schematic of sputtering principle.	28
Figure II. 3: Molecular beam epitaxy.	29
Figure II. 4: Schema of pulsed-laser deposition.	30
Figure II. 5: Dip-coating stages: (a) Immersion; (b) Start-up; (c) Deposition; (d) Drainage.	33
Figure II. 6: Schematic model describing the film formation of the spin-coating process.	33
Figure II. 7: General schematic of a spray pyrolysis deposition.	34
Figure II. 8: Steps of chemical vapor deposition technique.	35
Figure II. 9: Description of the desposition process initiated with increasing substrate temperature.	39
Figure II. 10: The spray pyrolysis setup.	40

Figure II. 11: Pneumatic spray nozzle.	41
Figure II. 12: The glass substrate.	42
Figure II. 13: Cut glass substrate using diamond point pen.	42
Figure II. 14: The furnace used to heat the substrate before deposition.	43
Figure II. 15: (a) Magnetic stirrer (b) Balance.	44
Figure II. 16: InCl_3 powder.	45
FigureII. 17: Steps of thin film preparation in pneumatic spray process.	46

Figures of Chapter III

Figure III. 1: schematic of x-rays diffraction according to Bragg.	48
Figure III. 2: X-ray diffraction equipment.	48
Figure III. 3: Full width at half maximum (FWHM) of an arbitrary peak.	49
Figure III. 4: variety of interaction products evolved due to interaction of primary electron beam and sample.	50
Figure III. 5: Photo of Scanning electron microscope.	51
Figure III. 6: Schematic of UV-Visible spectrophotometer.	52
Figure III. 7: UV-Visible Spectrophotometer.	52
Figure III. 8: XRD patterns In_2O_3 and $[\text{SmO}_3; \text{In}_2\text{O}_3]$.	53
Figure III. 9: SEM surface images of: a) pure In_2O_3 b) $\text{In}_{0.9}\text{Sm}_{0.1}\text{O}_3$ thin films.	56
Figure III. 10: Optical transmittance spectra of In_2O_3 thin films as a function of the wavelength.	57
Figure III. 11: Optical band gap spectra of pure indium oxide In_2O_3 .	58
Figure III. 12: optical band gap spectra of Sm doped Indium Oxide $[\text{SmO}_3; \text{In}_2\text{O}_3]$.	58
Figure III. 13: Energy versus density of states diagram for n- type degenerate semiconductor.	59

List of Tables

Table I. 1: Shows the number and positions of atoms forming the elemental cell of In_2O_3 .	17
Table III. 1: ASTM file of In_2O_3 .	54
Table III. 2: Shows the inter-planer spacing and lattice parameter a of the undoped and Sm doped In_2O_3 .	55
Table III. 3: Shows the crystalline size D of the undoped and Sm doped In_2O_3 thin films.	55

Abreviation

TCO:	Transparent Conducting Oxide
CBM:	Conduction Band Minimum
VBM:	Valence Band Maximum
REE:	Rare Earth Element
Sm:	Samarium
PVD:	Physical Vapor Desposition
CVD:	Chemical Vpaor Deposition
ALE:	Atomic Layer Epitaxy
PLD:	Pulsed Laser Deposition
MBE:	Molecuar Beam Epitaxy
CBD:	Chemical Bath Deposition
MOCVD:	Metal Organic Chemical Vapour Phase
PECVD:	Plasma-Enhanced Chemical Vapor Deposition
MF:	Mid- Frequency
RF:	Radio Frequency
DC:	Direct courant
UV:	Ultra violet
UHV:	Ultra High Vacuum
HEMT:	High Electron Mobility Transistors
SGDC:	SOL-GEL Dip Coating
SGSC:	SOL-GEL Spin Coating
YSZ:	Yttria Stabilized Zirconia
XRD:	X-rays diffractometer
SEM	Scanning electron microscopy

General Introduction

General introduction

With the current technological advanced research, thin films have been the center of numerous studies based on their interesting optical, electrical properties. Among thin films, transparent conducting oxide is the most studied material due to its optical and electrical properties[1].

(TCO)s are based on their wide bandgap($\geq 3\text{eV}$)[2] and defined by high electrical conductivity combined with low absorption rate in the visible region and great reflection in the infrared region. The most known is indium oxide(In_2O_3)[1], zinc oxide(ZnO)[3], and tin oxide (SnO_2)[4]. Based on their predominant charge carriers, TCOs may be divided into two categories[5]: p-type and n-type. The n-type TCOs, on the other hand, is the most widely accessible and, as a result, are more frequently used in practical applications[6].

Furthermore, Among the most used TCO materials, indium oxide (In_2O_3), thin-film has attracted much interest because of its direct wide bandgap of 3.5-3.75 eV and indirect bandgap of about 2.6 eV. It is cubic with the lattice constant of $a = 10.117\text{\AA}$ [7] and space group ($Ia\bar{3}$)[8], a dielectric constant of 8.9, and a refractive index of 2.0–2.1[9]. high transparency, chemical stability, mobility, and electrical conductivity. This unique combination of optical and electrical properties has promoted indium oxide thin films for extended applications, such as solar cells, heat-reflecting mirrors, antireflection coatings, gas sensors, and flat panel displays[5].

To the day, In_2O_3 thin films have been prepared by various thin-film deposition techniques such as spray pyrolysis, vacuum evaporation, magnetron sputtering, sol-gel method. Among these techniques, spray pyrolysis is a preferred technique; it is versatile to fabricate thin films, not expensive, commercially viable, easy, and simple to manipulate[10].

The overall aim of this study is to produce undoped and doped indium oxide films with acceptable characteristics for optoelectronic application, which may be utilized as transparent conductive oxide (TCO) thin films to minimize the losses during photovoltaic conversion through studying the structural, optical, and electrical properties of In_2O_3 film.

This thesis consists of four chapters organized as follows:

It started with a general introduction.

In the first chapter, we will explain the concept of thin films, background on transparent conducting oxides; we will present a bibliographical study of the fundamental physical properties (structural, optical, electrical) of indium oxide and their applications; in addition, we will give a brief introduction to rare earth generally and samarium precisely.

In the second chapter, we will describe various preparation techniques of films, and we will concentrate on the method of pneumatic spray pyrolysis, which has been used in this dissertation, followed by the experimental procedure and conditions.

The third chapter is titled characterization, results, and discussions, where we listed the characterization methods used for structural, morphological, and optical measurements. As we will explain and analyze the obtained results and give a general conclusion on them.

Chapter I

General concept

I.1 Introduction

Transparent conducting oxides (TCO) thin films are among the most important fields of current interest in material science. They have been extensively studied through the past years due to their essential potential technological applications, such as in flat-panel displays, solar cells, and other optoelectronic devices. Their exceptional properties, transparency in the visible spectral range, and low resistivity make them a unique material with higher aspects and desirable in the industry.

This chapter will present the definition of thin films, their type, and growth mode; then, we will mention transparent conductive oxides and their main properties and applications. Moreover, we will end this chapter by presenting a material description of indium oxide (In_2O_3) in its fundamental physical properties, namely crystallographic, optical and electrical, and rare earth.

I.2 Thin films

I.2.1 Definition

In concept, a thin film is an element of a given material deposited onto a substrate (Figure I.1), with reduced dimensions named thickness measured in angstrom. This quasi-two-dimensional (that is, the tiny distance surrounded by boundary surfaces) tends to cause the disturbance of most of the physical properties. When the thickness is much thinner, the emphasis on this quasi-two-dimensional appearance is more significant. However, as the thickness exceeds a specific threshold, the impact becomes smaller, as well as the material reverts to its well-known solid-material properties.

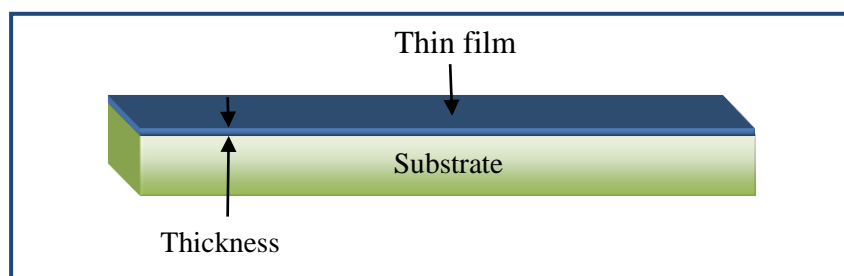


Figure I. 1: Schematic of thin-film deposited onto a substrate.

The main distinction between the material in the massive form and the one in thin layers is that: in the massive form, the functions of the limits in the properties typically are ignored. However, in a thin layer, these limits of properties functions are associate with the surface areas, wich are become predominant factors in a thin layer case [11].

The second essential characteristic of thin films is the deposition techniques; the thin film is always integrated with a substrate. As a result, it will be essential to include this important factor in the design of the deposition techniques, namely that the support significantly impacts the layer's structural qualities. Therefore, depending on whether it is deposited on an amorphous insulating substrate such as glass or a monocrystalline silicon substrate, where a thin layer of the same material with the same thickness may have very different physical characteristics [12].

I.2.2 Steps of the formation and the growth of thin-film using chemical vapor deposition technique

There are three main stages in every thin-film deposition process [12]:

- Creation of the deposit species.
- Transport of these species to the substrate.
- The adsorption of atoms on the substrate; and growth of the layers.

The formation of a thin film takes place through a combination of atomic processes, described as follows [13]:

a) Nucleation : the initial process for the creation of a stable nucleus, stated as follows:

Atoms arrived from the vapor initially generated (maybe assured by a molecular beam or the arrival of ions from solution) on the surface of the substrate and got accommodated at the surface as ad-atoms with bound energy E_{ads} [14]. At the highest temperatures, these ad-atoms will only remain on the surface for a brief moment [13]; there are two possible cases:

- **Desorption** (Figure I.2): the desorption occurs at the highest temperatures; in this case, the interaction of the atom-substrate is low, and the residence time is deficient; therefore, atoms will desorb via re-evaporation [14,15].

- **Adsorption** (Figure I.2): the adsorption phenomena take place at low temperatures; in comparison with desorption phenomena, the interaction of atoms-substrate is exceptionally high, and the adsorption residence time is powerful. Thus the atoms will stay much longer on the surface [15].

The desorption and adsorption are illustrated in Figure I.2:

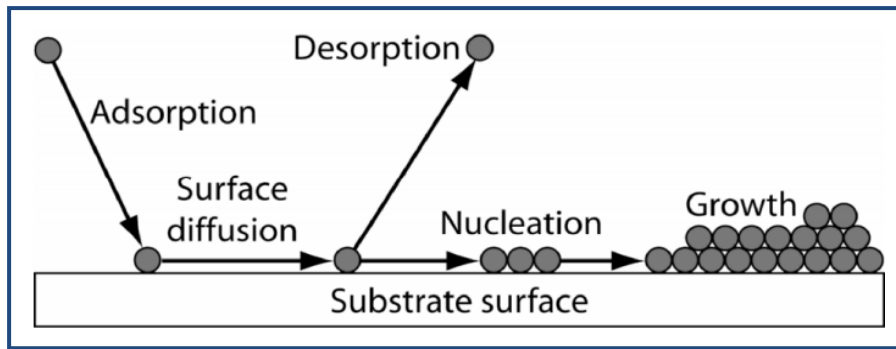


Figure I. 2: Adsorption, desorption and the nucleation process [16].

Initially, the adsorbed species are not in thermal equilibrium with the substrate, moving on its surface (diffuse over the surface). They will interact with each other during this diffusion, leading to aggregation of these single atoms generating clusters that will expand. Their stability depends on their size. The cluster must be more significant than a critical size so that it would be more stable. In this instance, the probability of germ growth is greater than the probability of its dissolution, as shown in Figure I.3 [12].

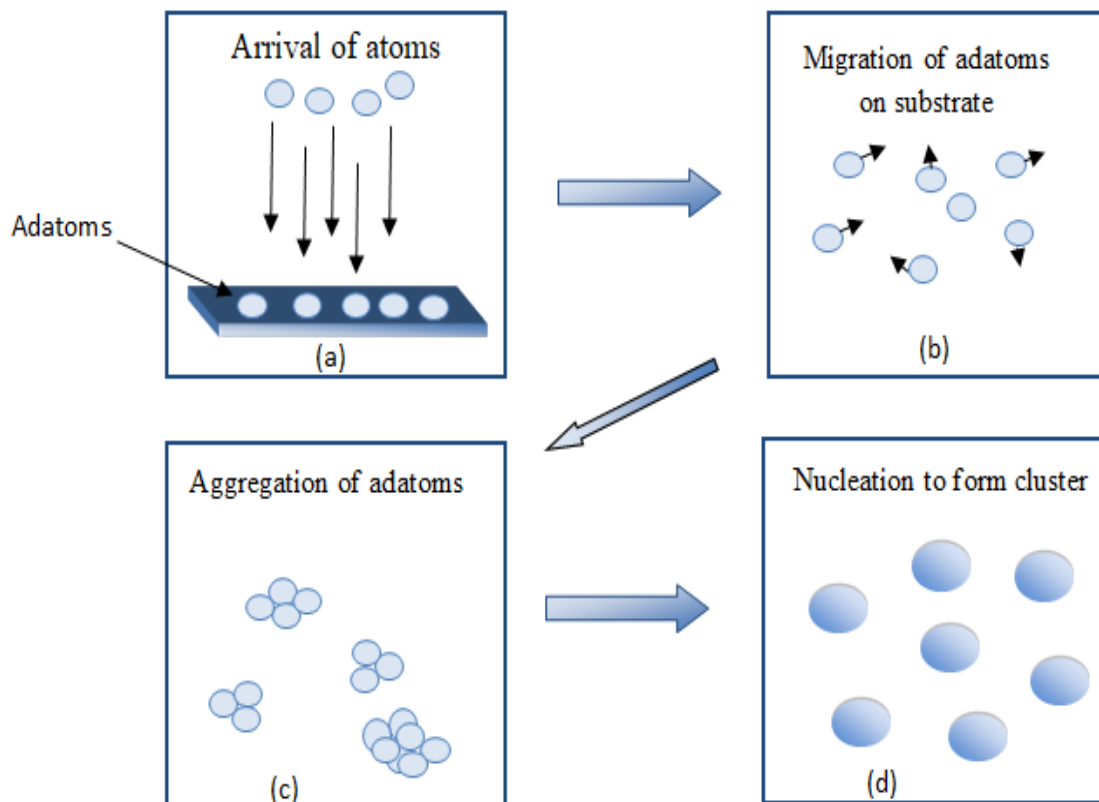


Figure I. 3: representation of thin- films nucleation:

- a) The arrival of atoms to the substrate. b) Migration of ad-atoms.
c) Aggregation of single ad-atoms. d) Nucleation.

b) Coalescence step

This step is the second stage of the growth process; it can follow different mechanics; it can be by the mobility of nanoparticles. Therefore, their diffusion on the surface leads to their collision and causes dynamic coalescence. The coalescence can also be achieved through a static coalescence, which will happen when two motionless nanoparticles, sufficiently close together grow, create an inter-diffusion zone between them, allowing a new, and larger cluster [17]. Furthermore, [Figure I.4](#) shows the process of coalescence:

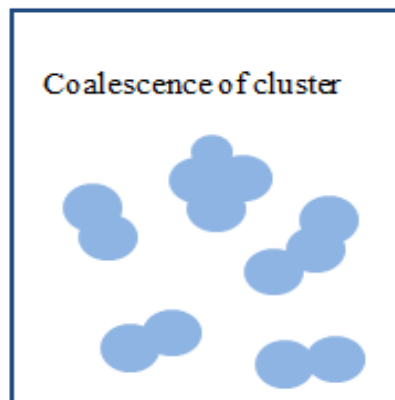


Figure I. 4: The process of coalescence.

c) Growth step

The cluster grows by the coalescence of sufficient grown clusters or the capture of ad-atoms in number and size until it attains nucleation saturation ([Figure I.5.a](#)). The nucleation of the cluster depends on several parameters such as the energy of the incident species, their quantity per unit of time and surface, the energies of activation, adsorption, desorption, thermal diffusion, the temperature, and the chemical nature of the substrate. An island may grow horizontal to the surface of the substrate by superficial dispersion of the absorbed or transverse spaces by the direct influence of the affected species on the islands.

According to surface energy and the relative values of atom-atom interaction energies of the fil, the growth can be two-dimensional (layer by layer) or three-dimensional (island) [18]. ([Figure I.5.b](#))

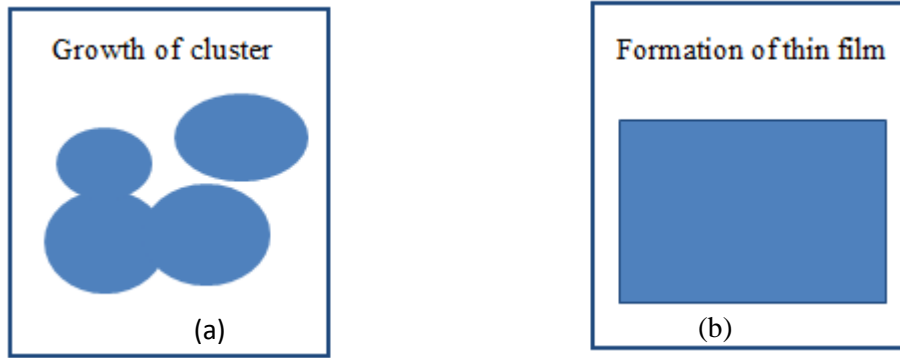


Figure I. 5: The process of growth and formation of the thin film.
 (a) Growth of cluster. (b) Formation of the thin film.

Generally, the lateral growth rate is substantially more significant than the perpendicular growth rate [12].

I.2.3 Thin film growth mode

There are typically three different modes of crystalline growth. We can distinguish between them by considering the relative magnitudes of the surface energies Γ_s , Γ_f of the substrate and the film, respectively, and the interfacial energy Γ_{in} [19,20]. They can be described as follows:

I.2.3.1 Layer type (called Frank and Van Der Merwe)

It is a bidimensional (2D) growth, occurs when $\Gamma_s \geq \Gamma_f + \Gamma_{in}$ the decrease in total system energy passes through the rise in the surface energy of the depot. In this case, the deposit will cover the whole substrate surface, and the growth is done layer by layer. In this mode, the adatoms-substrate interaction is powerful [21,15].

I.2.3.2 Islands type (called Volmer-Weber)

In this growth mode (3D), tiny nucleate clusters directly on the surface of the substrate and grow in islands on the substrate. These extend to produce islands that combine to create a continuous thin layer [21].

Island mode growth occurs when $\Gamma_s \leq \Gamma_f + \Gamma_{in}$ atoms or molecules that arrive on the surface of the substrate are more likely to bond with each other than with the substrate. As a result, the deposit will cover it only partially, and the growth will be on islands [22].

I.2.3.3 Mixed type (called Stransky-Krastanov)

The third mode of growth, called Stranski-Krastanov (SK), is a combination of the two previous modes: after a start of bi-dimensional growth (layer by layer), the deposited material may accumulate elastic energy (caused by lattice parameter conflict), which changes the value of Γ_s , Γ_f , and Γ_{in} . As a result, a shift in growth mode while the creation of islands becomes energetically favorable [23].

These modes are illustrated in the Figure I.6:

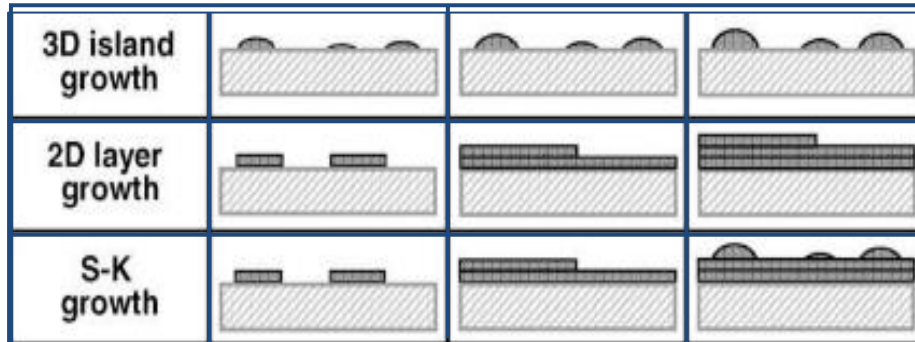


Figure I. 6: Illustration of the different modes [24].

Figure I.7 schematically illustrates the essential features leading to 2-D and 3-D nucleation on a substrate:

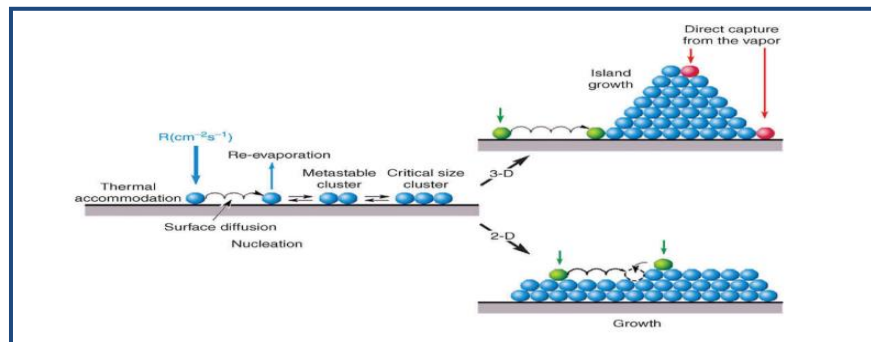


Figure I. 7: Schematic representation of processes leading to nucleation and 3-D (upper right) and 2-D (lower right) film growth [25].

I.3 Transparent conducting oxides

Because of the unique optoelectrical properties, transparent conducting oxides (TCOs) find many research and industry applications. TCOs thin-film fundamental features and applications are among the most significant areas of the current study of material science. They are an essential part of technologies that require large area electrical contact and optical access in the visible portion of the light spectrum.

TCOs thin films are a specific category of materials; they were discovered at the beginning of the twentieth century, when Baedeker deposited the first layer of cadmium oxides (CdO) inside a luminescent discharge chamber. He noticed that the thin layers were conductive and transparent at the same time. This observation gave birth to a new study area which remains a matter of reality after a long time [26,6].

I.3.1 Definition

Transparent conductive oxides (TCOs) are a specific category, precisely thin films containing one or two metallic elements; gather two main characteristics: high optical transparency in the visible light region~ over 85% merged with high electrical conductivity $10^3 \Omega\text{cm}^{-3}$ [4].

TCOs semiconductors are materials with a wide bandgap over 3.1eV that has a relatively high concentration of free electrons in the range of $[0.1 \times 10^{21} - 1.0 \times 10^{21} \text{ cm}^{-3}]$ in the conduction band and exhibit a low resistivity of order $10^{-4} \Omega.\text{cm}$, while being transparent in both the visible and IR portions of the electromagnetic spectrum because of the absorption of electromagnetic radiation which is caused by the high carrier concentration [2].

TCOs semiconductors have become the most widely studied because of their commercial value and essential technological applications, such as solar cells [20] and flat-panel [5]. The list of potential TCO materials has expanded to include In_2O_3 , Al-doped ZnO, GdInOx, SnO_2 , F-doped In_2O_3 , and many others [6].

I.3.2 TCOs properties

High optical transparency, good electrical conductivity, and mechanical durability are essential qualities that TCO must have; thus, the properties of TCO materials derive from the nature, number, atomic arrangements of metal cations in crystalline or amorphous oxide structures, and resident morphology [27]. Among the main properties of TCOs are:

I.3.2.1 Electrical properties

The semiconductors band theory can describe the electrical properties of transparent conducting oxides. Ground state electrons must be transported from the valence band to the conduction band minimum (CBM) through the bandgap after being excited by absorbing the photon's energy. TCOs are semiconductor materials with a wide gap ($E_g > 3.1 \text{ eV}$); high mobility

of $>65 \text{ cm}^2\text{v}^{-1}\text{s}^{-1}$ allows film resistivity in the low $10^{-4} \Omega\text{cm}$ range and requires degenerate carrier density $\geq 10^{20} \text{ cm}^{-3}$ [28,29].

a) Electrical conductivity

The conductivity σ expressed in ($\Omega^{-1}\text{cm}^{-1}$); is the product of the number of charge carriers in a material (N) and the mobility (μ) of these charge carriers times the elementary electron charge (e). Thus, the electrical conductivity is given by:

$$\sigma = N \cdot \mu \cdot e = \frac{1}{\rho} \quad (\text{I.1})$$

Where N: The number of charge carriers (cm^{-3}).

μ : The carrier charge mobility ($\text{cm}^2 \cdot \text{V}^{-1} \cdot \text{S}^{-1}$).

e: Electronic charge ($1.602 \times 10^{-19} \text{C}$).

Note that ρ is the resistivity, defined as the inverse of the conductivity(σ); in addition, its related to the charge carrier density and the carrier mobility if N increase; ρ will reduce [28].

TCOs materials are electrically conductive not simply due to intrinsic defects (oxygen vacancies or metal interstitials) but also due to an influence of their native defects such as defect complex and impurities, leading to the high unintentional carrier densities present in these materials [30].

b) Mobility

The mobility is a velocity of carriers (v) under unit electric field strength(E); as in (I.2) [2]:

$$\mu = \frac{v}{E} \quad (\text{I.2})$$

The mobility μ of an electron in semiconductors depends on the relaxation time (τ), the electronic charge (e) and the effective carrier mass (m^*) in the conduction band as given by the relationship (I.3) [28]:

$$\mu = \frac{e\tau}{m^*} \quad (\text{I.3})$$

As a result, the mobility will be increase by increasing τ or by decreasing m^* . Increasing τ requires films with fewer defects which may be accomplished by reducing carrier density, removing grain boundaries, and less neutral impurities [28].

The crystalline quality of TCO layers and grain size play a vital role in improving the mobility of charge carriers through heat treatment, choice of deposition technique, and the choice of the

substrate [28]. In addition, the mobility “ μ ” is limited by scattering the charge carriers in the lattice [29].

c) The effect of doping on TCO

By definition, doping is the introduction of impurities into a semiconductor crystal to improve its conductivity. Doping can be substitutional, creating vacancies, or interstitial implantation. We can distinguish two types of doping:

- **Doping n:** In n-type doping, the dopant atom replaces one of the host material's constituent atoms in bulk, resulting a non-bonding electron which creates a donor energy level close to that of the conduction band; this allows facile promotion from the donor energy level [31].
- **Doping p:** In p-type doping, the dopant atom creates an electronic deficiency in the ionic bonding, resulting in an empty acceptor energy level slightly above the valence band that can accept an electron from that valence band and leaves a positive 'hole' behind; this permits for conduction by moving a 'positive hole' through the material [31].

In general, the conductivity of n-type TCOs is always higher than that of p-type due to relative the small effective mass of electron in conduction band than that of the hole in the valence band.

I.3.2.2 Optical properties

Importance of optical property of TCO is due to a transmission window covering most of the visible range, which is defined by two imposed boundaries: One is in the near-UV region determined by the effective band gap E_g , which is blue-shifted due to the Burstein–Moss effect (Figure I.8). The other is at the near-infrared (NIR) region due to the increase in reflectance caused by the plasma resonance of the electron gas in the conduction band. The absorption coefficient α is very small within the defined window; therefore, transparency is very high [29,32].

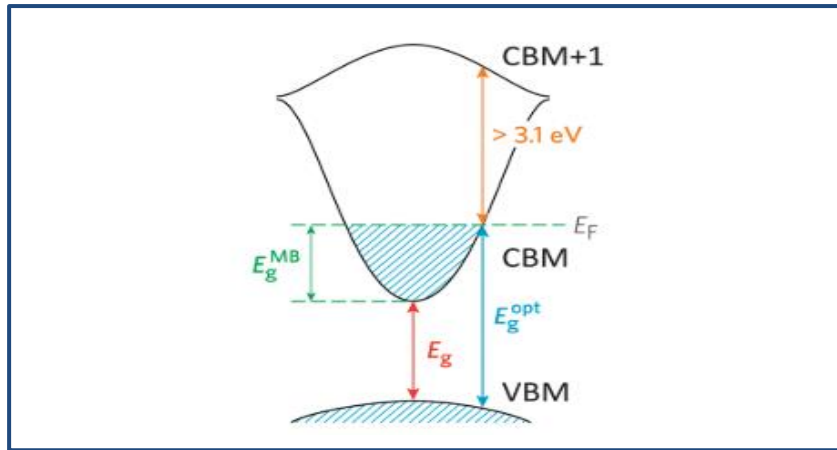


Figure I. 8: Diagram of the optical widening effect of the Moss-Burstein shift [33].

The principal factors that characterize the optical properties of TCOs are transmission factor T , reflection factor R , and absorption coefficient A . It is refractive index n , extinction coefficient k , band gap E_g and geometry (includes film thickness, thickness uniformity, and film surface roughness) that determines these factors [4].

• Transmittance factor T

An optical transmission is a dimensionless number defined by the ratio of transmitted light (Φ_T) and the intensity of the incident light at the surface (Φ_0) across the concerning material [34]:

$$T = \frac{\Phi_T}{\Phi_0} \quad (\text{I.4})$$

As we mentioned before, the important optical characteristic of TCOs is the existence of the transmission window in the visible region between near-IR and near-UV in the range $[0.4\mu\text{m} - 1.5\mu\text{m}]$ where no light is transmitted out of this range because of different phenomena [35].

- **Low wavelengths:** Where wavelengths are shorter than $0.4\mu\text{m}$ (in the near-UV), the absorption is achieved due to the fundamental band gap. The photon's energy is high regarding the band gap energy, as a result; this energy will be absorbed and transformed to the band transitions; thus, no light is transmitted, and that is due to the quantum phenomenon [35].
- **Longer wavelengths:** at a wavelength longer than $1.5\mu\text{m}$ (near-IR), reflection occurs due to the plasma edge, it can be described by the classical theory (Drude free electrons theory).

- **Reflectance factor R**

The reflectance factor R is a dimensionless number defined as the ratio of the light that is reflected at its surface (Φ_R) to the incident light intensity (Φ_0) [34].

$$R = \frac{\Phi_R}{\Phi_0} \quad (\text{I.5})$$

The films are characterized by high reflectance, up to 90%, which means films with lower carrier concentration do not exhibit the increase in reflectance characteristic of the plasma wavelengths [35].

- **Absorption coefficient**

The absorption coefficient is related to transmission and reflection by the Berr-Lambert relationship:

$$T = (1-R)e^{-\alpha d} \quad (\text{I.6})$$

Where T: transmission coefficient.

R: reflectance coefficient.

d: Thickness of the film.

α : absorption coefficient.

TCO thin films should have a very low absorption coefficient in the near UV-VIS-NIR region. The blue-shift of the edge of absorption in the near-UV region is associated with the increase in the carrier concentration blocking the lowest states (filled states) in the conduction band from absorption of photons [4,29,36].

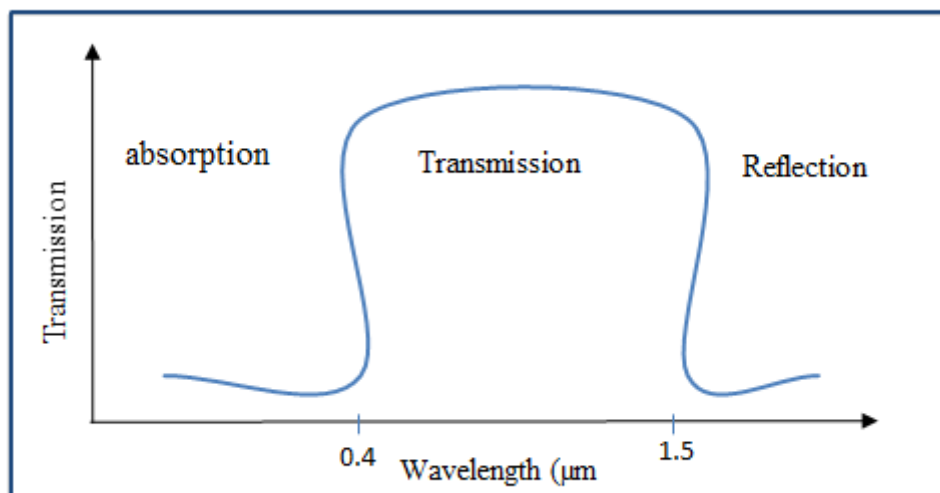


Figure I. 9: Transmission spectrum of TCOs.

I.3.3 Criteria for choosing TCO

Practically, many criteria influence the choice of a TCO, such as deposition method, non-toxicity, hardness of the layers, adhesion, thickness, deposition temperature, and manufacturing cost. The most suitable TCO is one that has good electrical conductivity with good optical transparency, as well as one that has a good merit factor. The quantitative assessment of the performance of a TCO is given by the quality Q , which is defined as the ratio of electrical conductivity σ to optical absorbance in the visible [37].

$$Q = \frac{\sigma}{\alpha} \quad (\text{I.7})$$

Where σ : Conductivity ($\Omega^{-1}\text{cm}^{-1}$).

α : absorption coefficient (cm^{-1}).

I.3.4 Application of TCO

Due to interesting of electrical and optical properties, TCOs have been attracted more intentionally in research and industry; the primary uses of TCOs are listed below:

- **Transparent heating elements:** can be used in aircraft and vehicular windshields as the defroster. TCOs can be used to make it; they have a significant advantage over conventional hot air blowers, quickly and evenly across vast regions [4].
- **Flat-panel display:** Generally, transparent electrodes are required for a wide range of electro-optical devices, such as flat panel displays and solar cells, the essential examples. In order to allow the backlight to pass through the liquid crystal film while providing voltage to the different pixel, TCOs are very needed and plays a vital role [4].
- **Solar cell:** TCO films are used as a transparent electrode in most solar cells. Besides conductivity and transparency, electrical compatibility with nearby layers in the cell, processing requirements, and environmental stability are all critical factors to consider when selecting a TCO for this application [4].

- **Coatings on architectural glass:** the reason for using coated windows in buildings is to control air condition in the summer and heating in the winter. TCO films are most commonly used to obtain these features mixing to unique properties; light transmission in the visible while reducing heat transmission [38].

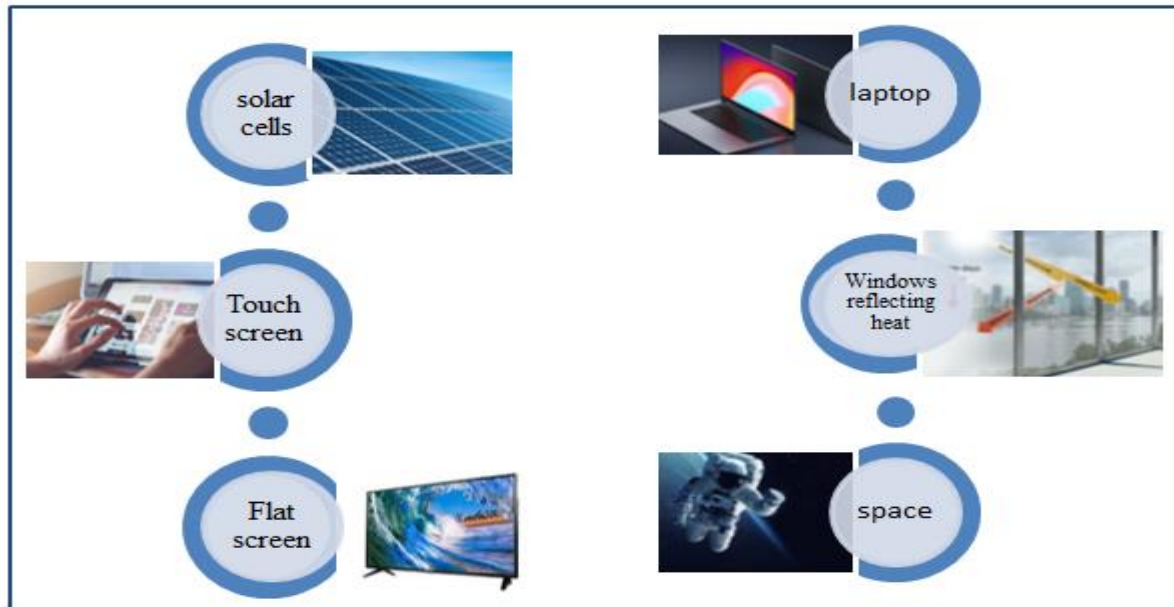


Figure I. 10: some applications of TCO [24].

I.4 Indium oxide

Indium oxide is an essential, highly degenerate n-type that exhibits electrical conductivity combined with high optical transparency oxide [39]. The optoelectrical properties of In_2O_3 films depend on their microstructure, stoichiometry, and impurity concentration [40]. In_2O_3 is physically stable and chemically inert [41,42]. It has a direct bandgap of 3.2 – 3.7 eV and an indirect bandgap of around 2.7 eV [43]. It could be an insulator in its stoichiometric form, while in its nonstoichiometric form behaves as a highly conducting semiconductor. Due to its double properties, high optical transparency, and good electrical conductivity, indium oxide thin film is commonly studied and it is most used in technological applications (TCO) [44–46].

I.4.1 Structural properties

Indium oxide (In_2O_3) is a yellow–grey crystal solid, while in the thin-film form, it is transparent and colorless [47]. Indium tin oxide (In_2O_3) has an estimated density of 7.12 g/cm^3 with a melting point of 1913°C [48]. It can crystallize in two different structures as centered cubic and hexagonal:

- **Centered cubic structure:** this structure exhibits a bixbyite cubic structure, similar to the structure of Mn_2O_3 (also called C-type rare earth sesquioxide structure [49]) with 16 unit molecules per unit cell, space group $Im\bar{3}$ and lattice parameter of $a = 1.012 \text{ nm}$ [50,51], which are represented in **Figure I.11** :

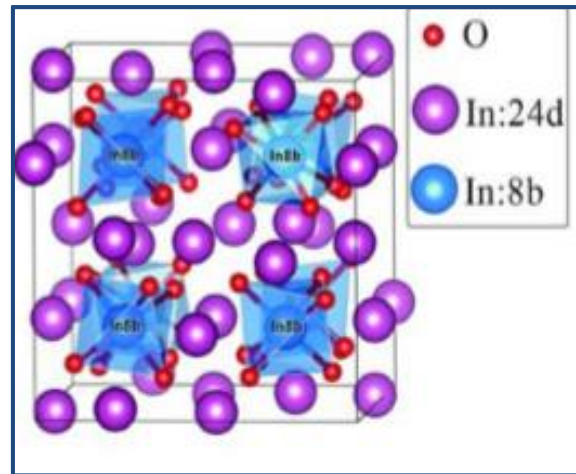


Figure I. 11: In_2O_3 bixbyite cubic structure [52].

Indium oxide structure is related to a $2 \times 2 \times 2$ supercell of fluorite, in which one-fourth of all anion sites are structurally vacant, providing for a bit of adjustment ($\approx 4\%$) of cations that surround them. There are 32 metallic atoms in the particular positions, of which are 8b and 24d sites in Wyckoff notation, forming two crystallographically nonequivalent indium atoms [45,46,53], shown in **Figure I.12**:

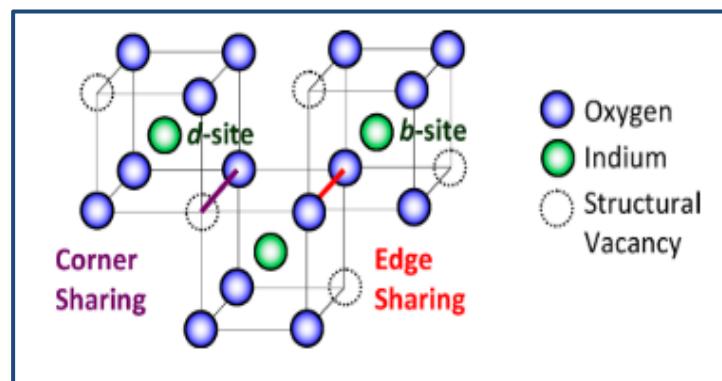


Figure I. 12: The coordination arrangement of In atoms [54].

- **Position In(1):** 1/4 of the In atoms (In1) occupy the centers of the trigonally distorted octahedra (8b position) [42]. Each Indium(1) atom occupies the center of a deformed cube, surrounded by six equidistant oxygen atoms at a distance of 2.188 \AA , with two body diagonally opposing corners vacant in the direction $\langle 111 \rangle$ [54]. as represented in **Figure I.13**.

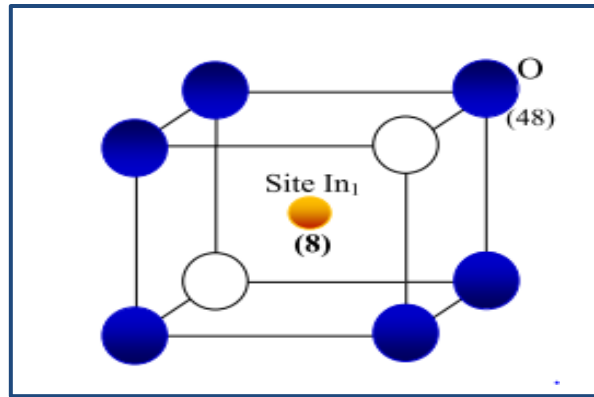


Figure I. 13: Schematic representation of the sites In(1) in the bixbyite structure of In_2O_3 [55].

- **Position In(2):** $\frac{3}{4}$ of In atoms (In2) occupy the centers of tetragonally distorted octahedra (24d position) [42]. Each Indium(2) is surrounded by six oxygen atoms which lie nearly at the corners of a cube, but in this case, two face diagonally opposite corners are unoccupied [52,50]. The 24b position exhibit less symmetry due to different sets of In-O distance, (2) 2.13 Å, (2) 2.19 Å, (2) 2.23 Å [54], as represented in Figure I.14.

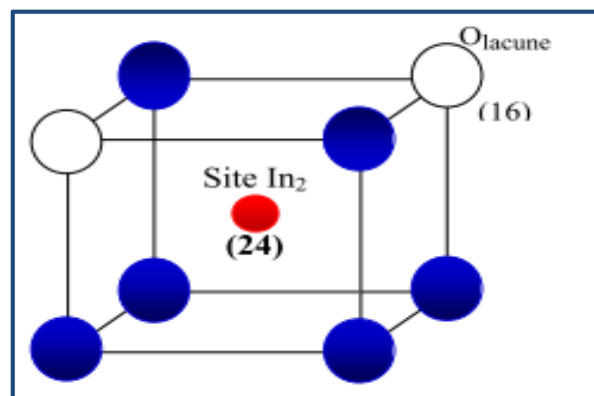


Figure I. 14: Schematic representation of the sites In(2) in the bixbyite structure of In_2O_3 [55].

When doping, $\frac{1}{4}$ of the doping atoms are on the In(1) sites and $\frac{3}{4}$ on the In(2) sites. The table below shows the number and positions of the 80 atoms forming the elemental cell of indium oxide [56]:

Table I. 1: Shows the number and positions of atoms forming the elemental cell of In_2O_3 [56].

Number	Atome	X	Y	Z
8	In(1)	$\frac{1}{4}$	$\frac{1}{4}$	$\frac{1}{4}$
48	In(2)	0.4668	0	$\frac{1}{4}$
48	O	0.3905	0.1529	0.3832

- Hexagonal structure:** Rhombohedral structure with space group $R\bar{3}c$ can be considered an arrangement of hexagonal close pack oxygens (Figure I.15), which is slightly distorted, and In^{3+} cations lie in two-thirds of the octahedral holes in the oxygen sublattice. The lattice parameters are $a = 5.49$ and $c = 14.52$. In this arrangement, the six coordinated In^{3+} cations are surrounded by three oxygens at a distance of 2.07 \AA and three in 2.27 \AA . It is similar to that of alumina α (corundum). It is produced either by high-pressure elaboration (for example, 65 kBar and 1000°C) or by adding metallic dopant [56–58].

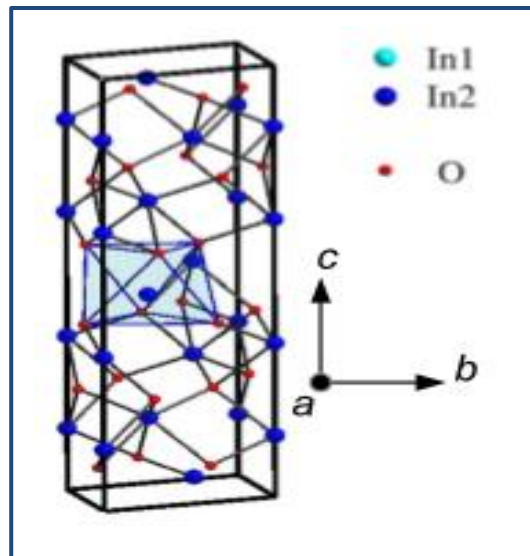
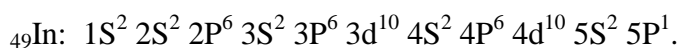
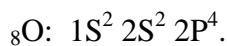


Figure I. 15: Rhombohedral polymorph structure of In_2O_3 [58].

I.4.2 Electrical properties

Indium oxide is an n-type, highly degenerated semiconductor material with a direct gap of about 3.6eV and an indirect bandgap around 2.5 eV . The high conductivity of the pure oxide layers is due to the high free carrier concentration (electrons) [59].

The electronic band structures of oxygen and Indium are:



Remarkably, the valence band of the semiconductor In_2O_3 is formed by the 2P states of oxygen, whereas the S states of Indium form the conduction zone. The bottom of the conduction band in In_2O_3 formed by a single free electron-like band of s-character hybridized with widely scattered O 2s states. The O 2p states hybridized with In 5d give rise to the valence band edge. This unique band structure causes a consistent charge distribution, which minimizes scattering to

a minimum. Moreover, the term of band dispersion can describe the increased electrical conductivity caused by mobility enhancement, and the Burstein– Moss shift [42,49].

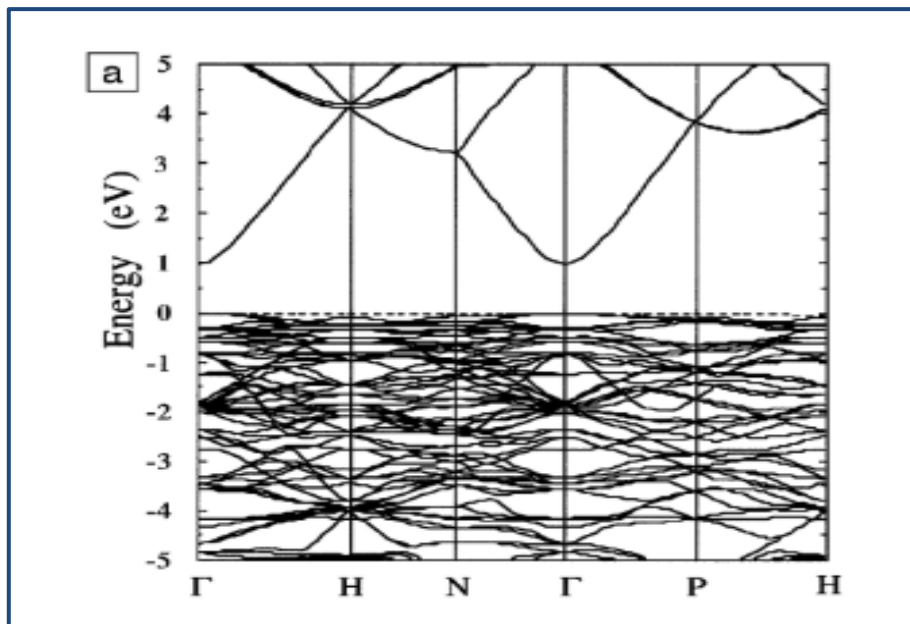


Figure I. 16: Electronic band structure of In₂O₃ [60].

Oxygen vacancies and interstitial doping atoms in the indium oxide crystal lattice are responsible for conduction phenomena in indium oxide films. Oxygen deficiency produces a nonstoichiometric or substoichiometric structure instead of stoichiometry (In³⁺)₂(O²⁻)₃. The conduction mechanism for the indium oxide system is typically explained by its defective chemistry [61-63].

In₂O₃ as a transparent conductor has higher mobility that varies in the range 10-75 cm² V⁻¹ s⁻¹, with an electron concentration $N \approx 10^{19}$ - 10^{20} cm⁻³, and a resistivity $\rho \geq 10^{-3}$ Ω cm [64,62]. These latest authors have shown that the best results are obtained after a reducing heat treatment that improves the conductivity.

I.4.3 Optical properties

The optical properties are strictly related to the band gap, transparent material must have a band gap energy greater than the energy of the visible light. This prevents electronic excitation from the conduction band to the valance band, and therefore maintains visible transparency in the material.

Indium oxide is a transparent material that has a direct band gap of about =3.7 eV (Erroneously, this value has been widely quoted as the fundamental band gap of In₂O₃) and

indirect band gap of 2.6 eV which allows high optical transparency at the visible rang of electromagnetic spectrum and strong optical absorption in the ultraviolet [43,58].

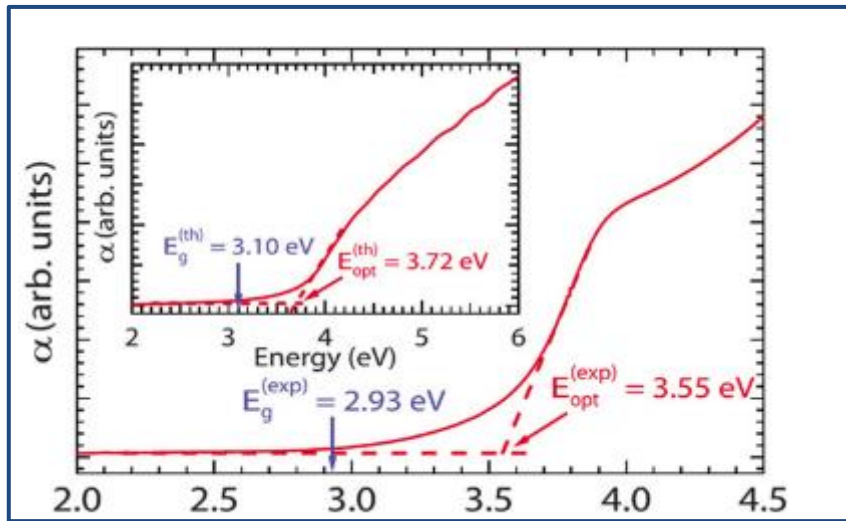


Figure I. 17: Optical absorption of In_2O_3 at ≈ 3.7 eV [58].

The optical band gap energy of In_2O_3 has been found to depend on various parameters like annealing temperature, oxidations conditions and the types of substrate used to grow the film. There are reports which suggest that the optical band gap of In_2O_3 thin films can be controlled by growth temperatures optimizing the way for growth temperatures to develop the high quality films and devices. It has also been figured that the growth temperature actually influence the structural, morphological, optical and electrical properties of In_2O_3 thin films and temperature is the most important parameter to grow high quality thin films [39,42,43].

I.4.4 Application of In_2O_3

Indium oxide thin films (In_2O_3) have a large variety of applications due to their unique properties, high optical transparency, and electrical conductivity such as: the microelectronic, optoelectronic, photovoltaic devices, transparent windows; liquid crystal displays (LCD), light-emitting diode (LED), solar cell, gas sensors, and anti-reflecting coatings and so on [8,65].

- **Gas sensors:**

Gas sensors are semiconductor material detectors of gases in the atmosphere at a low concentration such as CON , H_2S , H_2 , NH_3 , SO_2 , CO_2 , CH_4 and other hydrocarbons that can be harmful to human health. By definition, this device works directly at any interaction with an active gas and responds with an electrical signal due to the adsorption/ desorption after receiving a signal stimulus of the target gas. As a consequence, sensitivity, selectivity, and fast activity, in

addition, non-contaminating and lower operating temperatures, all these characteristics form an ideal gas sensor [66,67].

The gas sensor system works in two main parts [68]:

- **Sensing element:** it is the first essential part of the gas sensor working system for recognizing the gas at first contact (interaction).
- **Transducer:** the second step of the system which plays a role of transforming the interaction between the gas and the sensing element to an electrical.

The figure below show clearly the system of gas sensor:

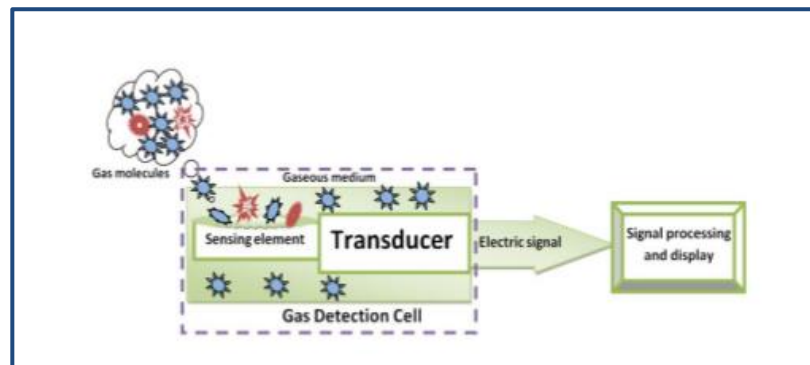


Figure I. 18: Schematic of chemical gas sensor [69].

The sensor should [61]:

- Operate continuously or at least in repeated cycles.
- Respond quickly.
- Be small and cheap.

In_2O_3 has a high sensitivity to the chemical environment, which makes it the most widely used for sensing applications. The oxygen vacancies on the surface, which is related to the electronic properties of In_2O_3 , govern the sensation process.

- **Windshields**

Indium oxide is lightly sprayed on the surface on many aircraft and high-end automobile windshields to provide a thin coating that protects against lower temperatures, effectively deicing the windshield and creating a frost-free travel experience.

- **Energy-Efficient Windows**

Using the same principles as the deiced windshields, indium tin oxide is also used to thinly coat the outside of many energy-efficient windows. The properties of indium tin oxide create a barrier that keeps cooler air outside.

- **Solar cells**

There has been interesting in recent years directed towards the development of conducting transparent oxide-based solar cells. These oxides provide the possibility of solar cells with performance characteristics appropriate for large-scale terrestrial application [70]. Transparent conducting oxides are particularly effective in solar cell application because of the following advantages

- a) The conducting transparent layer allows passage of solar radiation straight to the active area with little or no attenuation, such that solar cells based on these materials result in enhanced sensitivity in the high photon-energy part of the solar spectrum.
- b) Ease of manufacturing of the junction due to reduced junction formation temperature.
- c) These films may function simultaneously as low resistance contact to the junction and anti-reflective coating for the active region.

Besides, indium oxide can be used in different applications such as; transparent conductive electrode in electronic devices, liquid crystal displays, transparent conducting electrodes in flat panel displays and photo-detectors and different other optoelectronics applications[71].

I.5 Rare-earth

I.5.1 Generality

Rare-earth elements, also called rare-earth metals, were first discovered in 1794 by chemist and mineralogist Johan Gadolin, starting with the yttrium for the first time. At the end of the XIX century, chemists and mineralogists were able to research and identify a total of 14 elements of REE. In 1907, Lutetium and promethium were the last elements to be discovered; these two elements closed the history of the discovery of REE in the world [72].

The rare-earth elements are 17 metallic elements found in the middle of the periodic table [Figure I.19](#) divided into Lanthanides consists of 15 elements plus Scandium and Yttrium, which are considered rare-earth elements since they exhibit similar chemical properties and electrons structure [72].

A lanthanide is a group of elements ranging from atomic number 57 (Lanthanum) to 71 (Lutetium), having an atomic structure different from other elements. The Lanthanide term comes from the fact that they are all remarkably similar to Lanthanum. The other two rare-earth, Scandium and yttrium, are not part of the Lanthanide series and will be treated separately [73].

The similarity in characteristics of the lanthanides series includes [73]:

- The Similarity in physical properties throughout the series.
- Crystalline compounds usually have a 3+ oxidation state, although some can also have a 2+ or 4+ oxidation state.
- Coordination numbers in combinations are generally greater than 6.
- Across the series, the coordination number decreases.
- They bind preferably with high electronegative elements such as oxygen or fluorine.

The image shows Mendeleev's Periodic Table of Elements. A red box highlights the rare earth elements, which are the lanthanide series (elements 57-71) and the actinide series (elements 89-103). The table includes various annotations such as 'Table of Common Polyatomic Ions', 'Element categories', and 'State of matter at 25 °C'. The rare earth elements are located in the f-block at the bottom of the table.

Figure I. 19: Rare earth element (red box) in mendieiev periodic table [74].

Some rare earth elements have unusual magnetic, luminescent, and electrical properties that make them valuable for industrial applications and manufactured products [72].

I.5.2 Common properties of the rare-earth

- The rare earth elements are silver, silvery-white, or grey metals.
- The metals have a high lustre but tarnish readily in the air.
- The metals have high electrical conductivity.
- There are minimal differences in solubility and complex formation between the rare-earth.
- The rare earth metals naturally occur together in minerals.
- Rare earth is found with non-metals, usually in the 3+ oxidation state.

I.5.3 Atomic structure

The lanthanides (the elements La–Lu) possess filled f-orbitals, which have seven sub-orbitals. Each suborbital holds two electrons. Consequently, there are 15 different ways to occupy the f-orbitals, resulting in 15 other Lanthanide elements. These elements have very

similar characteristics except of cerium (which also produces 4^+ ions) and europium, ytterbium, and samarium, which all create 2^+ ions; the lanthanides are all trivalent (3^+) [73].

Scandium and yttrium, both considered rare earth elements (due to their chemical similarities), have a $3+$ oxidation state [73].

I.5.4 Samarium chloride

Samarium chloride (SmCl_3) is an inorganic compound. It is a white solid that desolves quickly in water to become $\text{SmCl}_3 \cdot 6\text{H}_2\text{O}$ forming a hexahydrate. Samarium chloride (SmCl_3) has an estimated density of 2.383 g/cm^3 with a melting 682°C .

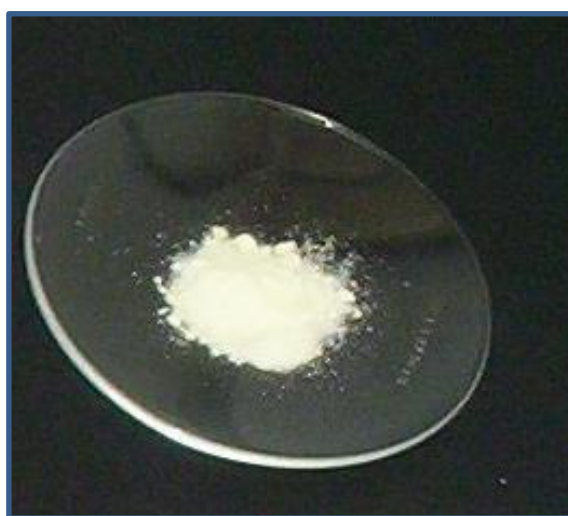


Figure I. 20: Samarium (III) chloride hexahydrate.

The crystal structure of SmCl_3 has been determined to be hexagonal, space group $P6_3/m$. SmCl_3 crystallises in the UCl_3 motif. The Sm^{3+} centres are nine-coordinate, occupying trigonal prismatic sites with additional chloride ligands occupying the three square faces

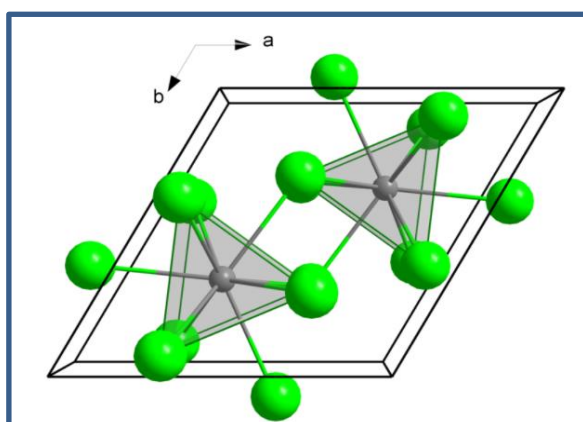


Figure I. 21: Crystal structure of SmCl_3 .

Conclusion

This chapter defines the thin film and explains the formation and thin film growth steps. Followed by an explanation of transparent conducting oxides and their properties and range of application. At the end of the chapter, we presented a bibliographic study of indium oxide, which illustrated the structural, optical and electrical properties and brief bibliographic of rare earth.

Chapter II

Thin films : Elaboration techniques

II.1 Introduction

Throughout the years, numerous techniques have been created to produce thin films, and that is due to their technological importance and scientific curiosity. Usually, the same material deposited by two distinct methods has different physical properties because the growth method generally plays a significant role in controlling thin film properties since the electrical and optical properties of the films depend strongly on the structure, morphology, and nature of the films impurities that present.

Thin-film deposition techniques can be classified into physical and chemical deposition processes based on the nature of the employed methods. In the physical processes, during the deposition; the provided material is physically deposited onto the substrate, include physical vapor deposition (PVD), pulsed laser, thermal evaporation, and sputtering; while the chemical methods are based on chemical reactions between precursors, include two principal categories gas phase and liquid phase deposition methods. The gas-phase methods are widely used, such as chemical vapor deposition (CVD) and atomic layer epitaxy (ALE). While spray pyrolysis, sol-gel, electrodeposition, spin coating, and dip-coating are liquid phase methods. The thin film deposition technics are summarized in Figure II.1:

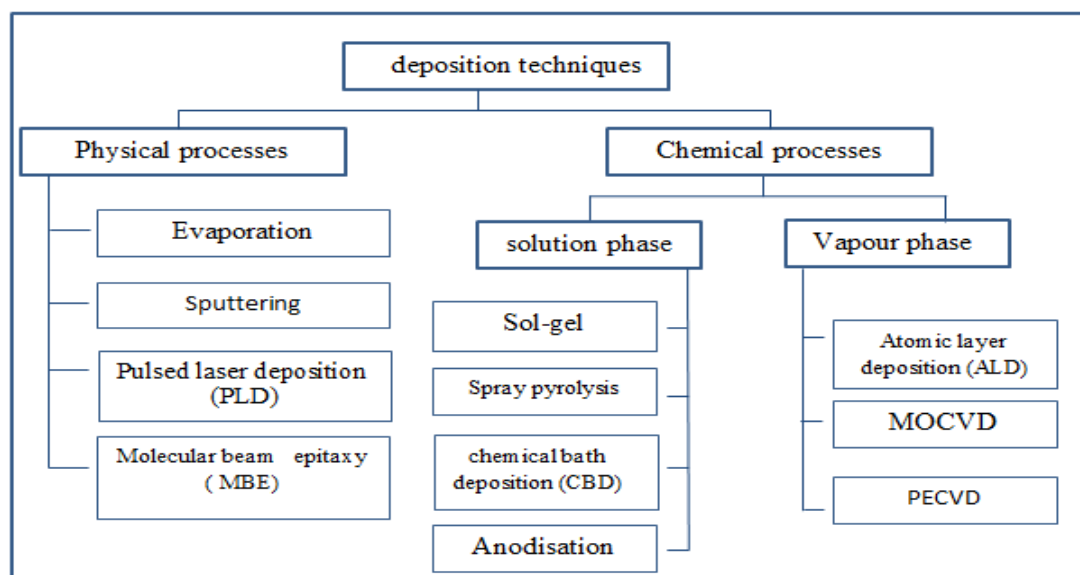


Figure II. 1: The classification of thin film deposition methods.

There is no universal technique for producing thin films, since each one of them has benefits and disadvantages. To improve the quality of the treated films, many methods were generated to enhance the benefits and minimize the negatives.

Section 1: Elaboration techniques

II.2 Physical deposition processes

Physical deposition methods mainly including evaporation, spraying in all its forms and pulsed laser beams. The most widely used PVD methods are molecular beam epitaxy and sputtering.

The production of thin films using physical processes occurs along the following sequence of steps:

- a) Physical evaporation of the deposited material.
- b) Transporting the resulting vapor phase through a low-pressure area to the substance.
- c) The vapor species condense on the substrate to form the thin film.

II.2.1 Sputtering

Sputtering is a high vacuum-based coating method that belongs to physical vapor deposition (PVD) processes defined as the ejection of particles (atoms, ions) used to deposit different materials such as metals, refractory materials, dielectrics, and ceramics. Also, it was used to produce an oxide metal layer by controlling the crystalline structure and surface roughness. This technique can use single-target or multi-target, which plays the role of the cathode that carries the substance or compounds to be deposited [75].

The concept of the sputtering technique is to bombard the surface of the target attached to a cooled electrode (the cathode) and placed it into a vacuum chamber. The target is bombarded using the energy of a plasma (partially ionized gas) to extract the atoms of the substance surface one by one and deposit them on the substrate that plays the role of the anode (it is an electrode positioned parallel to the target, at a distance of a few millimeters). The plasma is created by ionizing a pure gas, usually its Argon, by providing a potential difference (Pulsed DC) or electromagnetic excitation (MF, RF) between the cathode and the anode (a voltage of few KV), at relatively high pressures (10^{-1} - 10^{-3} mbr) starting from a lower pressure before the introduction of Argon to prevent any contamination due to the remaining gases. Because of the existence of the electromagnetic field, the Ar^+ ions are accelerated and confined around the target [76,77]. [Figure II.2](#) shows a schematic diagram of the sputtering technique:

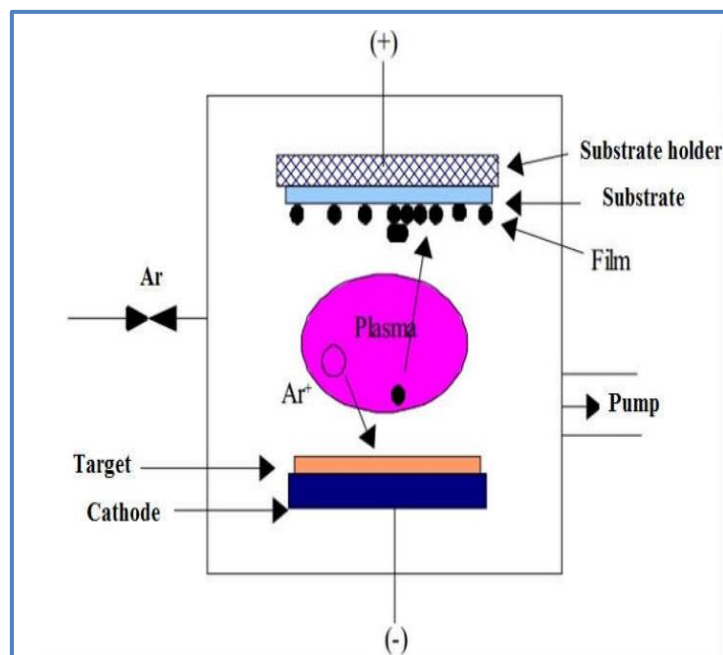


Figure II. 2: Basic schematic of sputtering principle [78].

There are two types of sputtering [76]:

- Simple sputtering: if the atmosphere (gas) of the discharge is neutral.
- Reactive sputtering: if it consists of the active gases such as oxygen O₂ or nitrogen N₂.

Depending on the mode of creation of the plasma and the nature of the target (conductive or insulating), we can distinguish two types of cathodic sputtering: direct cathodic sputtering (DC) only in the case of the sputtering of conductive materials and sputtering radiofrequency (RF) which allows the spraying of conductive materials or insulating materials [79].

Many factors affect the deposition process, including base vacuum, sputter gas pressure, sputter power, target, and substrate temperature [77].

The sputtering technique has so many advantages, such as the ability to produce high-quality thin films. Furthermore, the possibility to deposit a wide variety of metals, insulators, alloys, replicating of the target composition in the deposited film. In addition, this technique can in-situ cleaning before film deposition by reversing the potential on the electrodes [75].

The main disadvantage of the sputtering technique is the substrate damage due to ion bombardment or UV generated by plasma, and the deposition rate of some materials is quite low. Moreover, difficult to deposit uniformly on complex shapes such as turbine blades. Besides, most of the energy incident on the target becomes heat, which must be removed [75].

II.2.2 Molecular Beam Epitaxy (MBE)

The molecular beam epitaxy (MBE) is an experimental technique used for the layer-by-layer growth of thin films based on the reaction of molecular or atomic beams with a heated crystalline substrate, performed in an ultra-high vacuum (UHV) environment. Because of its possibility of producing homoepitaxial material at low temperatures (400-600°C for silicon), this technique was developed to grow semiconductors such as GaAs, CdTe, ZnSe. In addition, to provide time for the arriving atoms into the surface through surface diffusion to crystallographic sites at low epitaxial temperatures, it is essential to operate slowly [80].

This technique consists of transmitting molecular jets to the surface of a substrate previously chosen to achieve epitaxial growth (oriented growth) in a deep vacuum (typically 10^{-10} Torr), to avoid any impact or contamination on the path and to produce a nearly atomically clean surface, and that is by evaporation via the heating source of material to be desposited to melting point using joule effect(resistive wire), radiation (knudsen cell) or electronic bombardment (electron cannon). By controlling the evaporation cells and under UHV, the free average distance traversed by each atom is highly long; in this case, the atoms travel in a straight lines without any shock; as a resulting a jet of molecules is ceated towards the substrate which is usually silicon or gallium arsenide [80,81].

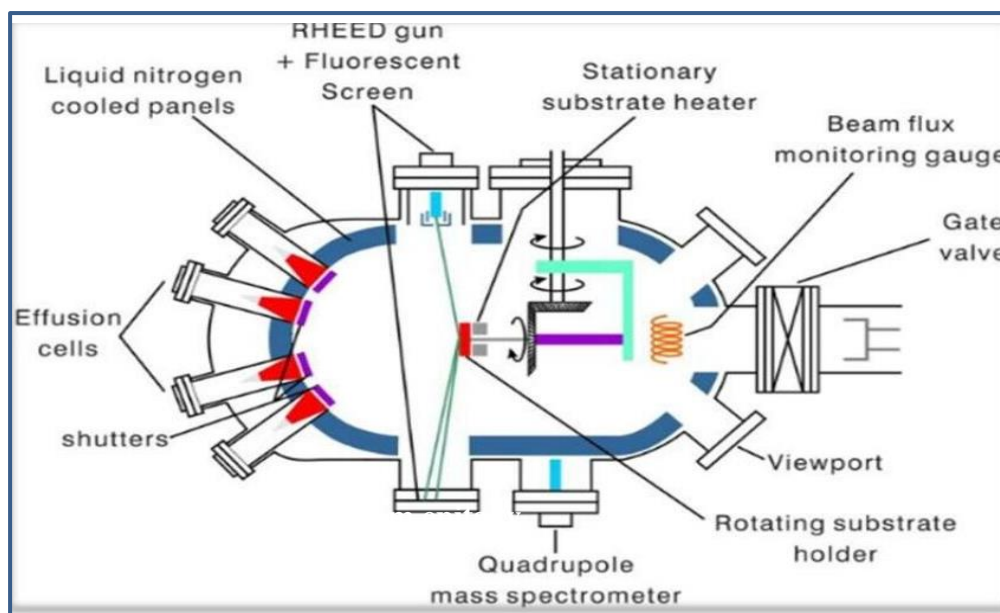


Figure II. 3: Molecular beam epitaxy [82]

MBE can be used to produce very complex structures such as laser diodes, and the super-lattice molecular beam is widely used to manufacture nanotechnologies. It is

extensively employed to produce semiconductor devices, including high electron mobility transistors (HEMT) [81].

Among the advantages of the molecular beam epitaxy method is the possibility of doping with different rates of impurities due to a low growth rate. Furthermore, it has the ability to control the thickness of tiny layers with extreme precision. The MBE technique's disadvantage is the complexity of the apparatus and the difficulty of incorporating a high vapor-pressure source.

II.2.3 Pulsed laser deposition

Pulsed laser deposition (PLD) is a technique that belongs to physical vapor deposition (PVD), in which a laser (Nd, YAG, or other similar lasers) with a high power density and limited frequency bandwidth and these types of lasers are used to vaporize the target material. With a controlled chemical composition; this technique can be utilized to deposit high-quality thin films, alloys, and compounds [83,84].

Generally, the principle of this technique is simple: it is based on the projection of an intense pulsed laser beam focused on the surface of a target. This last consists of the deposited material on the substrate and placed in an ultra-high vacuum chamber. Based on a specific power density provided to the target, a significant amount of material is extracted from the target with spatial distribution in the form of a dense luminous plasma plume that expands rapidly away from the target surface to be collected on a substrate placed at a short distance from the target [85,86]. The figure underneath illustrates the fundamental principle of the PLD.

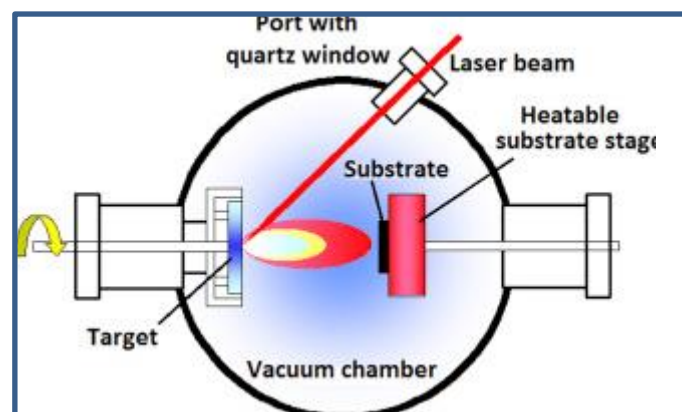


Figure II. 4: Schema of pulsed-laser deposition [87].

The deposit nature and quality depend on several parameters such as the plasma properties of the plume, energy of the laser, the nature and pressure of residual gas in the enclosure. In addition, it is necessary to control the transport of the species of the target [87].

➤ **Advantage**

- Conceptually simple: a laser beam vaporizes a target surface, producing a film with the same composition as the target
- Versatile: many materials can be deposited in a wide variety of gases over a broad range of gas pressures.
- Cost-effective: one laser can serve many vacuum systems.
- Fast: high quality samples can be grown reliably in 10 or 15 minutes.

➤ **Inconveniences**

- Thickness deposition is not uniform.
- For the overall perfect and pure film, it is necessary to maintain a very low pressure of the order of 10^{-10} torr, which is slightly difficult.
- This process is very expensive as compared to CVD process.
- The growth rate is very small compared to the growth rate in CVD process.

II.3 Chemical Deposition process

The Chemical deposition is a method in which liquid precursors react to form a solid deposit. The main interest of chemical deposition is its simplicity and ease of controlling elaboration conditions.

The construction of the thin layers by this method follows three steps:

- Preparation of the solution.
- Cleaning of the substrates.
- Start drawing on the substrate (the deposit).

II.3.1 Sol-Gel

The Sol-Gel technique is an ideal and cost-effective approach for producing thin films among several chemical deposition varieties in solution. As its name implies, the Sol-Gel method allows the produce of thin films via the development of a colloidal suspension (Sol) and polycondensation of the Sol to produce a wet gel (Sol-Gel).

The fundamental concept of the Sol-Gel process is simple: a combination of liquid precursors is converted into a solid through a low-temperature using a polymerization-type chemical reaction to hydrolysis and condensation [88].

The Sol-Gel process includes the following steps:

- **Making a Sol:** The starting solution consists of a molecular precursor, a solvent (usual alcohol), water and sometimes a catalyst (acid or basic). The chemical characteristics of the precursor then determine the choice of solvent or catalyst. Finally, each component is dosed very precisely.
- **Gelling the Sol:** It is described as the point at which the entire solid mass turns interconnected. This step could be done on a substrate in order to produce a thin film or in-mold [88].
- **Drying:** During the final phases of polycondensation, water and the organic solvent are evaporated from the glass cavities, and the volume of the solid matrix decreases progressively [88].

There are two paths of sol-gel synthesis, which are [89]:

- **Inorganic or colloidal:** obtained from metallic salts (chlorides, nitrates, oxychlorides) in an aqueous solution [89].
- **Metallo-organic or polymeric:** obtained from metallic alkoxides in organic solutions [89].

There are two methods of depositing thin layers in the solution:

a) Dip-coating (SGDC)

It is a deposition technique that to produce transparent oxide films with exceptional homogeneity and surface quality. First, the solution is distributed by immersing the substrate in a precursor material bath and extracting it under highly regulated and steady circumstances. Next, the deposition is pyrolyzed to remove all the organic compounds, finally dried by allowing the solvent to evaporate, leaving behind a solid polymer layer. This process is repeated many times until the required thickness is achieved [10,90].

The dip-coating process can be summarized in five steps presented in Figure II.5:

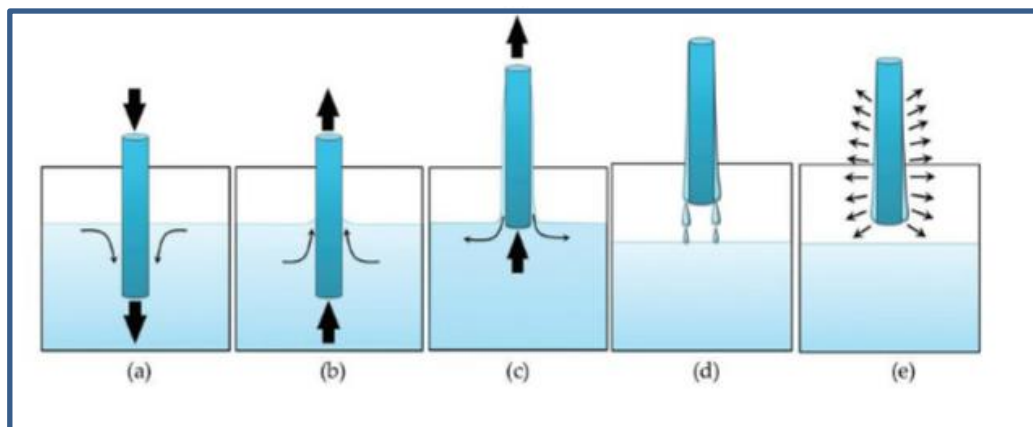


Figure II. 5: Dip-coating stages: (a) Immersion; (b) Start-up; (c) Deposition; (d) Drainage [48].

b) Spin-coating

Sol-Gel method using spin coating approach is a technique for depositing thin films on flat surfaces that are homogeneous in thickness. It is a centrifuge-based deposit technique. The precursor deposit into the center of a spinning substrate, The centrifugal force permits the substance to spread uniformly over the whole surface of the substrate due to the rotation. The thickness of the film is determined by: the rotation speed of the screwdriver, acceleration, and duration [91,92].

The Spin-coating process can be summarized in four steps presented in Figure II.6

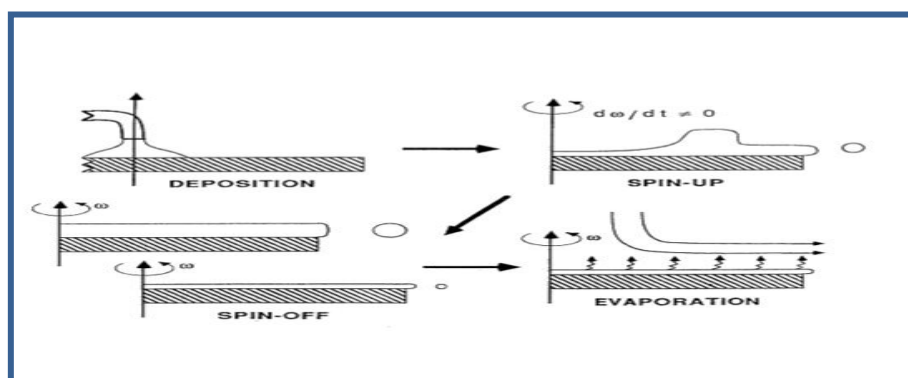


Figure II. 6: Schematic model describing the film formation of the spin-coating process [48]

Among the advantages of the Sol-Gel technique is producing thin films with excellent adhesion. In addition, this technique has the ability to produce a thick film for the protection against corrosion.

Besides, it can synthesize high-purity products [48]. The main inconveniences of this technique are that it takes a long processing time, high cost of raw materials [48,91–93].

II.3.2 Spray pyrolysis

Spray pyrolysis is the most frequent method utilized nowadays due to its ability to create an extensive range of thin films, conducting and semiconducting materials. This method aims to use an atomizer to spray and project a solution of two reactive chemicals onto a heated surface, where a chemical process leads to the formation of a thin layer after the volatile components of the reaction. The substrate temperature provides the energy required to initiate the chemical reaction between the solution components [94,95]. Figure II.7 shows the schematic of the spray pyrolysis process.

The thin film formation by the pyrolysis spray can be summarized by two simple steps: droplet formation at the end of the spout and decomposition of the precursor solution on the heated substrate.

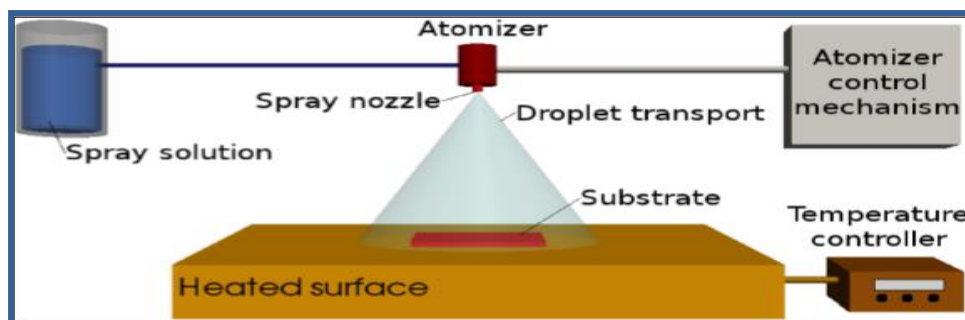


Figure II. 7: General schematic of a spray pyrolysis deposition [90].

"Spray pyrolysis" is the most popular name for this method. It consists of pyrolysis and spray[96].

- **Pyrolysis:** signifies the heating of the substrate. The essential role of the temperature of the substrate is to provide the necessary energy to start the chemical reaction, called activation energy [96].
- **Spray:** It refers to the jet of delicate liquid droplets which are launched by a sprayer. The atomization process determines the droplet size; for example, aerosol produces larger droplets, where in ultrasonic spraying produces smaller initial droplets [96].

The simplicity of this technique is the most important benefit; unlike most other thin layer deposit techniques, it does not need a pumping system. We choose this technique to

deposit our samples. In the second part of this chapter we will go through in-depth this technique [97].

II.3.3 Chemical Vapor Deposition(CVD)

Among the gas phase deposits, chemical vapor phase deposition (CVD) is an important technique and the most widely used method for developing and producing a thin film of semiconductor material. CVD is a technique for depositing a solid layer on a heated substrate based on a chemical reaction of one or more gas-phase components. The temperature is necessary to activate the chemical reaction of precursors just over the heating substrate to create thin layers. Generally, the volatile components of the substance to be deposited are diluted in a carrier gas and delivered into an enclosure containing the substrates [93,94], as showing in Figure II.8.

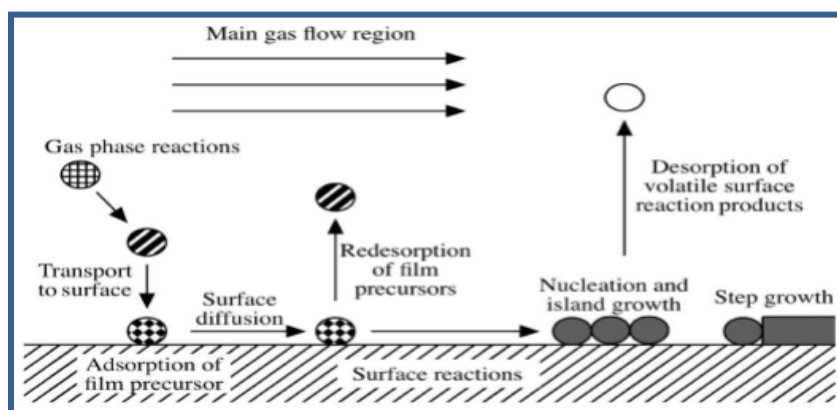


Figure II. 8: Steps of chemical vapor deposition technique [98].

The main parameters to control during the CVD disposition are the nature and temperature of the substrate, the chemical composition of the starting products, the gas flows (reactive and dilution), the overall pressure, temperature, and the shape (geometry) of the reaction chamber [99].

The main advantages of this method are: it is used to manufacture different thin layers, and on various substrates, the controlling of composition during deposition is possible, and it produces a uniform thickness with excellent adhesion, the ability to obtain deposits on complex forms and without needing a deep vacuum is possible. Generally, it is a low-cost technique[98,100,101]. On the other hand, the principal disadvantages of this technique: are the substrate deformation caused by the temperature gradient and the migration of impurities from the heated substrate [56].

Section 2: Experimental procedure (protocol)

II.4 Choosing the technique

As we stated in the previous part, the properties of thin films are strongly related to the used technique; therefore, several factors should be considered for selecting the appropriate deposition to utilize to get better results, which include the following [102]:

- Straightforward and relatively cost-effective method.
- A straightforward technique for preparing thin layers of different compositions.
- A technique that does not require high-quality substrates or chemicals.
- A technique that can be used to deposit thick, porous films, powder production.

Among the chemical methods, we chose the pneumatic spray pyrolysis technique as part of our study. This deposition technique is easy, cost-effective, and a considerable range of precursors may be utilized. In addition, the precursor solution can adjust the composition of the film and for other reasons, as follow [94,95,103]:

- It is an attractive technique for film deposition with high uniformity and across a large area.
- It is a simple method and maybe (can be) inexpensive.
- It is a method developed for the deposition of conductive oxides and the applications of solar cells.
- This technique can deposit dense and porous structures.
- Different types of atomizers can be part of spray pyrolysis equipment.

II.5 Pneumatic spray pyrolysis technique

II.5.1 Working principle

This method consists of spraying a droplet of a solution containing different compound constituents, and finely this droplet is atomized by a carrier of air just above a heated substrate on which precursors react. The objective of the heated substrate is to activate the chemical reaction between the reactive compound and the substrate to form a film. Droplets are formed after spraying and projected using aerosol or atomizer [104]. The experiment is usually performed in a normal atmosphere [105]. However, it may be performed in a vacuum chamber of the order 502 Torr [104–106].

Typically, the thickness of deposit thin films using this technique depends on the concentration of the precursor, the volume of the solution to be sprayed, and the deposition duration.

The process of creating thin films using the pyrolysis spray technique may be divided into three steps:

- **Generation of the aerosol:** droplet formation at the end of the spout.
- **Transportation of the aerosol:** transportation of sprayed species to the substrate.
- Decomposition of the precursor solution on the heated substrate.

II.5.2 Atomizer modes

An atomizer is a professional device characterized by its low beam beak called a nozzle that allows obtaining fine spray droplets and distributes them in the air. Several atomization methods have been employed for solution aerosol production, including pneumatic, ultrasonic [107–109], and electrostatic [110–112]. The main difference between these atomizers is the droplet size, rate of atomization, and velocity of droplets.

Because the pneumatic spray pyrolysis technique was used in this investigation, we suggest highlighting its characters in the next paragraph.

a) Pneumatic spray

This technique requires a precursor solution and heated substrate as well as an atomizer. In this mode of atomization, the solution is atomized as small drops, and these droplets are then transported to the heated substrate due to a carrier air. The pneumatic spray is a highly efficient, cost-effective, and easy to apply method. Besides, the thin films generated have a high surface area of substrate covering and mass synthesis potential and uniformity. On the other hand, Spray pyrolysis seems to be ineffective due to the poor thin film quality, heat breakdown, and vapor convection. The vapors are produced as a result of a temperature differential that prevents the source from adhering to the substrate [113, 114].

II.5.3 Processing steps of pneumatic spray pyrolysis technique

A solution of different reactive chemicals is sprayed on a heated substrate using an atomizer. The formation of a thin layer can be divided into three main steps:

- The spraying of the solution.
- The transport and solvent evaporation.

- Diffusion and precursor decomposition on the substrate.

The experience may be done in the air and can be prepared in a vacuum enclosure (around 50 Torr).

II.5.3.1 Atomization of precursor solution

This process happens when the flow of the solution contacts with air pressure at the lower end of the nozzle (spout) [104].

For a long time, liquid atomization has been intensively studied. It is crucial to understand the fundamental atomization mechanism. The key is to know which kind of atomizer is more suitable for such an application and how the performance of the atomizer is affected by liquid properties and operating conditions [103].

II.5.3.2 Aerosol transport

The transport of the generated droplets is the second important step in the spray process. During the deposition, the pulverized can be transported under pressure from the nozzle to substrate; this mode of conduction has two advantages: the flow can be controlled with great sensitivity, and the gases can be used as reactive elements in the composition of the material to be deposited. The most commonly used inert gases are argon and nitrogen. Some droplets stay in the air during aerosol transmission, while others evaporate into powder, producing the thin layer to be deposited [108,68].

The homogeneity of the deposited material can be determined by the size of the spray droplets and the solution concentration. At the same time, the concentration and droplets velocity generated by the atomizers can also be used to identify their morphology [112].

II.5.3.3 Precursor decomposition

When droplets reach the heated surface of the substrate, several processes occur simultaneously: evaporation of the remaining solvent, droplet dispersion, and salt decomposition. The authors, Viguié and Spitz, suggested the processes shown in [Figure II.9](#), which occur when the substrate temperature rises [108].

➤ In the low temperature regime (process A)

Aerosol droplets are projected directly onto the surface of the substrate and decompose. In this temperature range, the result of aerosol processes reaches the surface of the substrate

as the liquid state, which spreads the droplet along the surface. This evaporation is too late during the growth process. This low-temperature range produces layers that can be thick and therefore arise the absorbency, rough or non-adhesive, and cracks may appear.

➤ **At higher temperatures (process B)**

In this case, the solvent evaporates entirely during the flight of the droplet, and dry precipitate hits the substrate, where the decomposition occurs. This process promises layers that can be dense and with excellent adhesion to the substrate.

➤ **At even higher temperatures (process C)**

Before the droplet reaches the surface, the solvent evaporates. Then the solid precipitate vaporizes and goes into the gaseous phase without decomposition. The vapor that is produced during this process will be adsorbed and diffused into the surface to undergo a chemical reaction to form the layers. This process results in dense films with excellent adhesion.

➤ **At the highest temperatures (process D)**

In this process, the evaporation of the precursor occurs before reaching the substrate, and consequently, the solid particles are formed after the chemical reaction in the vapor phase.

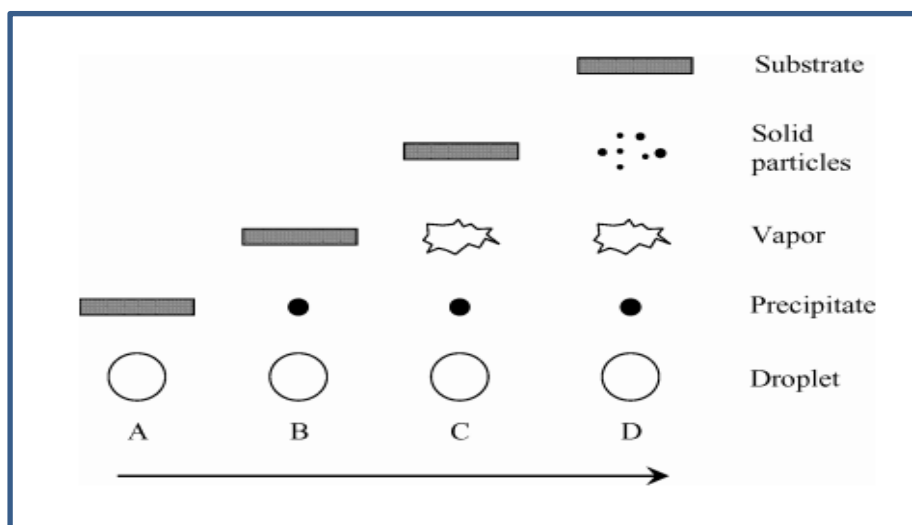


Figure II. 9: Description of the desposition process initiated with increasing substrate temperature[108].

II.5.4 Advantages of spray pyrolysis technique

Spray pyrolysis is ahead popularity due to its cheap cost, and it is increasingly being utilized in commercial applications such as the deposition of a transparent layer on glass

[111]. The deposition of a yttria stabilized zirconia (YSZ) layer for solar cell applications [108], anodes for lithium-ion batteries [115], and optoelectronic devices [113].

The main advantages of spray pyrolysis techniques are:

- Easy control of composition and microstructure (simple method to dope material by adding doping ingredient to the spray solution).
- Deposition at moderate temperatures of 100-500°C.
- Spray pyrolysis is cost-effective and can be easily performed.
- Substrates with complex geometries can be coated.

II.6 Experimental procedure

II.6.1 Used montage

The experimental montage used is pneumatic spray pyrolysis (Figure II.10) in the laboratory of (Procédés pour Matériaux, Energie, Eau et Environnement) at the University of Bouira to prepare the pure In_2O_3 and In_2O_3 doped Sm_2O_3 thin film.

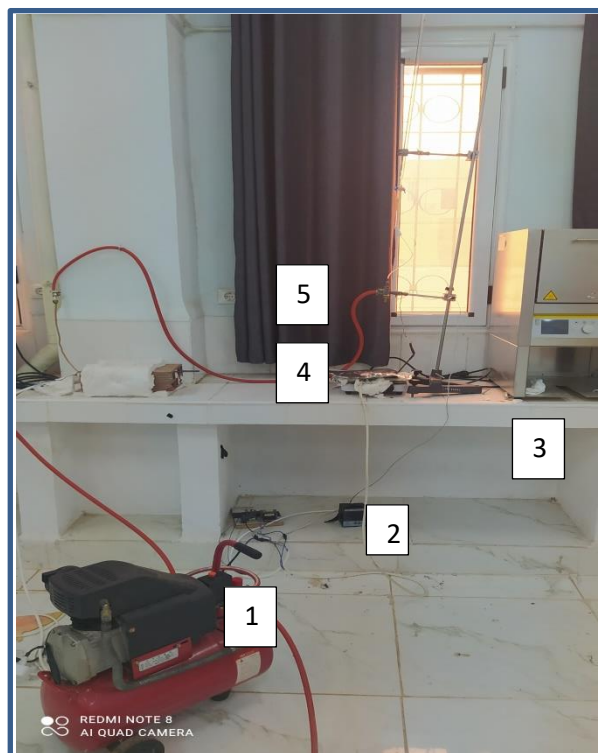


Figure II. 10: The spray pyrolysis setup.

- 1- compersor.
- 2- temperature regulator related to a thermocouple to control the temperature.
- 3- Thermocouple.
- 4- resistance.

5- Pneumatic spray nozzle.

Our work aims to create a system of thin layers using pneumatic spray technology, which is constructed from simple pieces with a few modifications that have been made to make homogeneous films. It consists of a pneumatic spray nozzle (see Figure II.11), substrate heater, automatic temperature control unit, air compressor, thermocouple. The heater is a stainless metal block furnace electrically controlled by an automatic temperature controller unit to attain the required substrate temperature with an accuracy of $\pm 5^{\circ}\text{C}$; the resulting temperature on the surface of the substrate is measured with a chrom-alum thermocouple. The pneumatic spray nozzle was fixed at an appropriate distance from the substrate.



Figure II. 11: Pneumatic spray nozzle.

II.6.2 The choice of the substrate

The thin film properties depend strongly on the state of the substrate and the preparation of its surface. The deposition process is directly influenced by the roughness, chemical properties, and surface energy.

The indium oxide films (In_2O_3) studied are deposited on glass substrates (solid glass). The choice of glass as a deposition substrate has been adopted due to the following reasons:

- ❖ It appears good thermal expansion with In_2O_3 ($\alpha_{\text{In}_2\text{O}_3} = -20.10^{-7} \text{ }^{\circ}\text{C}^{-1}$, $\alpha_{\text{verre}} = 85.10^{-7} \text{ K}^{-1}$), which minimizes the constraints at the substrate-layer interface and good adhesion.
- ❖ It offers excellent transparency, and this character is indispensable for films that are designed to work in the visible region.
- ❖ Economic reasons.

The substrates used are made of solid glass (MICRO SOLID) of dimensions (7 x 2.5 cm²) with a thickness of 1 mm from SAIL brand that presents a resistivity of 10²⁰ Ω.cm at room temperature.



Figure II. 12: The glass substrate.

II.6.3 Preparation of the substrate

As previously stated, the purity and surface state of the used substrate determine the quality of indium oxide thin films. The process of preparing the substrate and cleaning its surface is stated as follows:

1. Firstly, cut the substrate to a squared surface of (2.5 x 2.5 cm²) using a diamond point pen as shown in the following figure:



Figure II. 13: Cut glass substrate using diamond point pen.

2. Cleaning the substrate

The state of the substrate surface strongly influences the properties of the deposited films and, in particular, on homogeneity and adhesion. Therefore, before the deposition operation, cleaning the substrate surface is essential to remove all different contaminants covering the surface (greases, dust, fingerprints, impurities) to obtain adequate adhesion and good quality films. The substrates undergo cleaning decontamination of the surface according to the following steps:

- ❖ Cleaning the substrate with ethanol for 15 min.
- ❖ Clean with a distilled water in bath submitted to ultrasonic for 15 min at room temperature to eliminate the traces of greases and impurities.
- ❖ Cleaning the substrate using acetone for 15 min.
- ❖ Rinsing with distilled water for 15 min.
- ❖ Washing in methanol during 15 min.
- ❖ Rinsing with distilled water for 15min.
- ❖ Drying the substrate using optical paper.

3. Heating the substrate

The substrate can be damaged during deposition due to the difference of temperature between the sprayed solution and the heated substrate, leading to a thermal shock. So, it is necessary to prepare the substrate to hold up against any changes in temperature and increase the performance. To do that, we will put the substrate inside the furnace (Figure II.14) at a temperature of 150°C for 1 hour.



Figure II. 14: The furnace used to heat the substrate before deposition.

II.6.4 Preparation of the solution (precursor)

The precursor solution was prepared using indium chloride (III) dissolved in ethanol (C_2H_6O) with a molar concentration 0.2 mol/l. The precursor was prepared by taking fixed amount of indium chloride ($m= 1.76$ g) calculated by the equation (II.1) into a fixed volume of ethanol ($V= 40$ ml). The solution was then stirred for 2h using a magnetic stirrer (see Figure II.15.a) at $60^\circ C$ to yield a clear and transparent.

The mass of the salt used is calculated by the following expression:

$$m_{\text{precursor}} = \frac{C.M.V_0}{1000} \quad (\text{II.1})$$

With $m_{\text{precursor}}$: necessary mass for V_0 of precursor.

C: solution concentration (molarity).

M: molar mass of precursor.

V_0 : used volume.

The doped solution was prepared by adding to the precedent solution ($Sm_2Cl_3,6H_2O$) as doping source. The solution was then stirred for 2h using a magnetic stirrer (see Figure II.15.a) at $60^\circ C$ to yield a clear and transparent.



(a)



(b)

Figure II. 15: (a) Magnetic stirrer (b) Balance.

- **Ethanol:**
 - ✓ Aspect: liquid.
 - ✓ Color: colorless.
 - ✓ PH: neutral (20°C).
 - ✓ Melting point: – 117°C.
 - ✓ Boiling point: 78°C.
 - ✓ Dynamic viscosity: (20°C) 1,2 mPa*s.
 - ✓ Temperature of auto combustion: 425°C.
 - ✓ Point flash: 12°C .
 - ✓ Vapor pressure: (20°C) 59 mbar.
 - ✓ Density: 0,79 g/cm.
- **indium chloride:**
 - ✓ Purity: 99.99% .
 - ✓ Aspect: white crystal (dissolve in water).
 - ✓ Density: 3.46g/cm³.
 - ✓ Melting point: 586 °C.



Figure II. 16: InCl₃ powder.

II.6.5 Experimental conditions

In this work we prepared two series of solution pure and doped with fixed all parameters of deposition that can influence the characteristics of our samples.

- Solution flux rate: * ml/min
- Temperature: 420°C.
- Distance (nozzle-substrate): 18cm.
- Solution concentration: 0.2 mol/l.

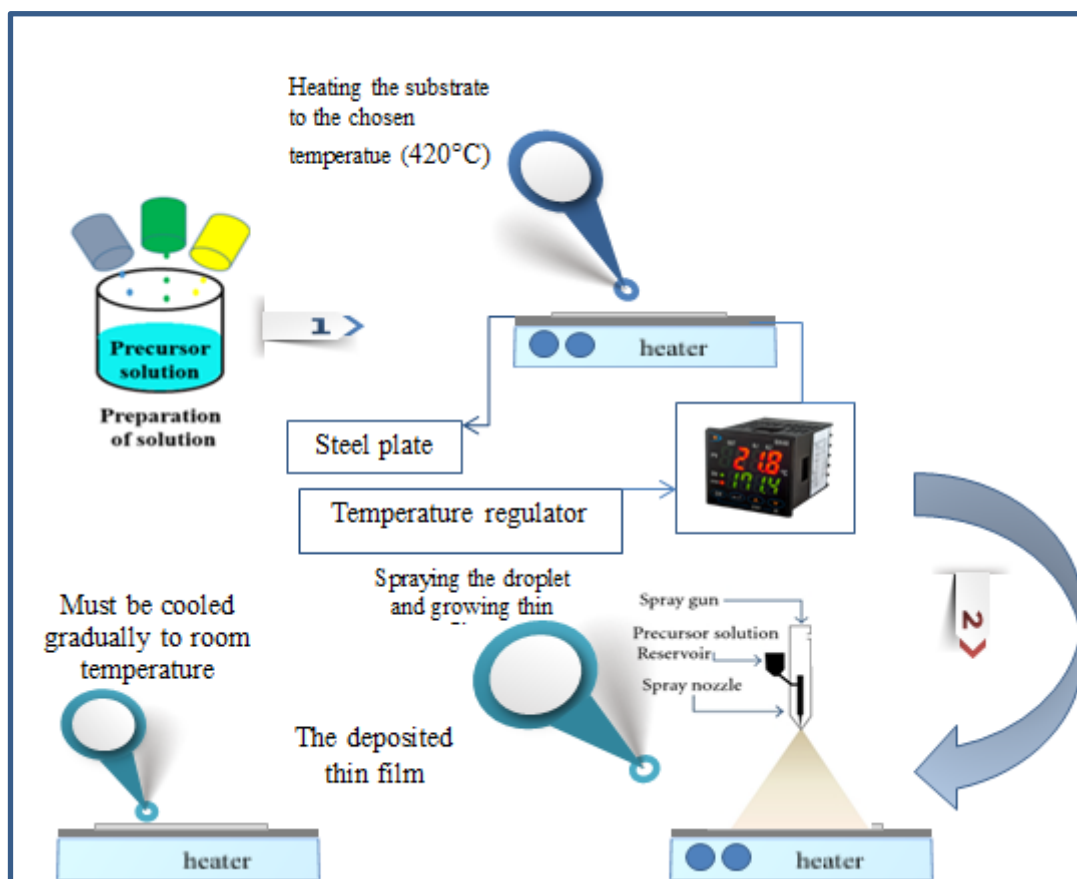
- Deposition time: 4 min.
- Solution quantity: 40 ml.

II.6.6 Deposition process

The deposition procedure undergoes several steps after preparing the substrate and the solution, which are stated as follows:

We shall place the substrate above a resistance whose feed is connected to a temperature regulator. The substrate will be heated gradually to the chosen temperature (in our case, 420°C) to avoid the thermal shock. After reaching the necessary temperature and fixing the flow of the solution and the distance (substrate-nozzle), very fine droplets are sprayed vertically on the heated substrate leading to the formation of a thin layer and the solvent evaporates due to the endothermic reaction.

At the end of depositing the layer, we must wait until the substrates are cooled gradually to room temperature in order to avoid the thermal shock that could break the glass.



FigureII. 17: Steps of thin film preparation in pneumatic spray process.

Chapter III

Characterization, Results and Discussion.

III.1 Characterization methods

Many techniques were used to characterize the obtained thin-film layers such as X-rays diffraction, Scanning electronic microscopy (SEM), and UV-Vis spectroscopy. In this section, we expose the principal of these techniques. In addition, we discuss the obtained results.

III.1.1 X-rays diffractometer (XRD)

X-ray diffraction is the oldest and most powerful method used to characterize the structure of the materials. With a greater penetration depth of 10 μm and a depth resolution of 200 \AA , this technique can provide much information about the crystal structure, preferred orientation of polycrystals, lattice parameter, crystallite, and stresses [116].

Two critical advantages of X-ray diffraction for thin film analysis are [116]:

- The wavelengths of X-rays are of the order of atomic distances in condensed matter, which qualifies their use as structural probes.
- X-ray scattering techniques are non-destructive and leave the investigated sample intact.

Traditionally, X-rays are radiation electromagnetic with photon energies in the range 100 eV- 100 KeV. Only short wavelengths from several angstroms to 0.1 angstroms (hard X-rays) are used in X-ray diffraction applications. Because the wavelength of X-rays is comparable to the atomic dimension, and they can penetrate deep into the material, they are used to provide information on the crystalline structure, especially the size and orientation of crystalline.

a) X-ray diffractometer principal

The basis of this technique is the interaction of monochromatic X-rays beam emitted by a source with the sample to be analyzed. Diffraction occurs when light is scattered by a periodic array with long-range order, producing constructive interference at specific angles. It is regarded that electrons in an atom coherently scatter light acting as a point scattering source. The scattering factor is proportional to the electron number surrounding the atom. XRD analysis is performed by a collimated beam of wavelength X-rays typically between 0.7 - 2 \AA incident on a specimen surface. The wavelength of X-rays is comparable to the spacing between atoms. The beam is diffracted by the crystalline phases in the specimen according to Bragg's law as shown in equation (III.1) [116] and illustrated in [Figure III.1](#):

$$2d\sin\theta = n\lambda \quad (\text{III.1})$$

Where d is the spacing between atomic planes in the crystalline phase, and λ is the X-ray wavelength. The intensity of the diffracted X-rays is measured as a function of the diffraction angle 2θ and the specimen's orientation [116].

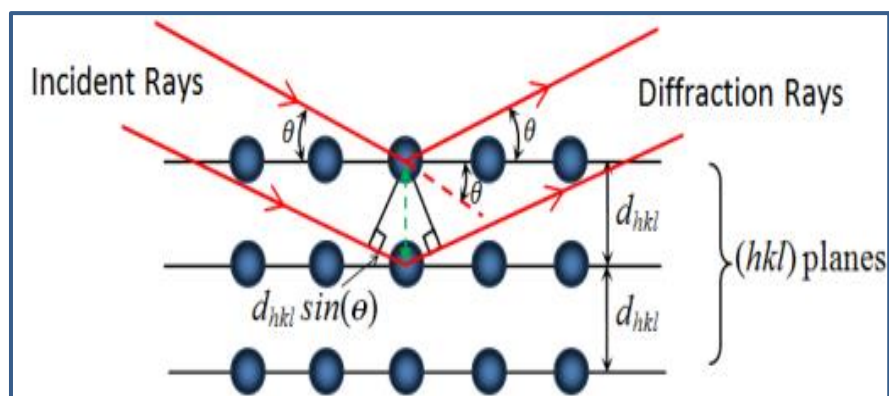


Figure III. 1: schematic of x-rays diffraction according to Bragg [69].

The diffraction patterns obtained experimentally of the sample are compared with the standard patterns in the international tables of the JCPDS-ICDD¹. Based on this comparison, we can establish the diffracted planes and the orientation of the sample.

As part of our work, we used a diffractometer (Figure III.2) Siemens D8 advanced. X-rays are produced from a λ CuK α radiation source, with a wavelength of 1.541838 Å, with an acceleration voltage of 30 kV and a current of 40 mA. The scan was done in steps, between 10° and 120°.



Figure III. 2: X-ray diffraction equipment.

¹ **JCPDS-ICDD:** Joint Committee of Powder Diffraction Standard International Centre for Diffraction Data.

b) Information obtained from the X-ray Diffractogram

There is much information that we can deduce from the X-ray diffractogram, some of which are presented below

- **grains size**

From the X-ray diffraction pattern, the width generated in a peak which known as the full width at half maximum (FWHM) (See Figure III.3), can be used to calculate mean crystallites sizes of the film in a direction perpendicular to the respective (hkl) planes, by using the Scherer's formula[116], [117], which is given as:

$$D_{hkl} = \frac{0.9\lambda}{\beta_{hkl} \cos \theta_{hkl}} \quad (\text{III.2})$$

Where (D_{hkl}) is the average grain size obtaining from the peak (hkl), (λ) is the wavelength of the X-ray beam, (β_{hkl}) is the full width at half maximum intensity of the peak (hkl) and (θ_{hkl}) is the angle between the incident ray and the (hkl) scattering planes.

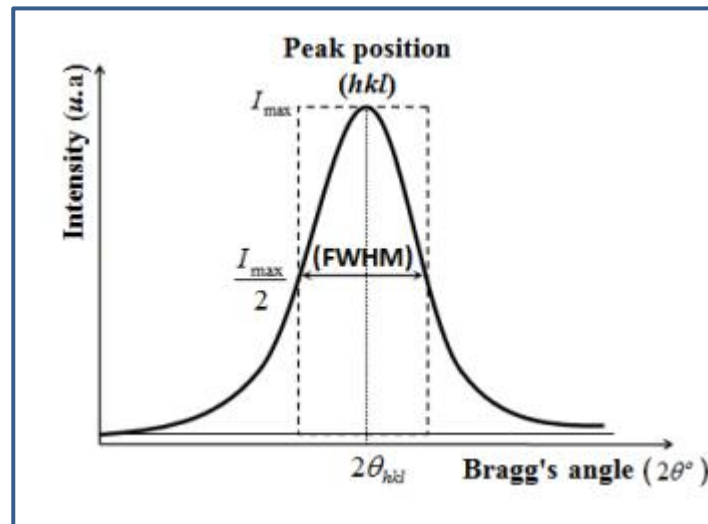


Figure III. 3: Full width at half maximum (FWHM) of an arbitrary peak [69].

- **Lattice parameters**

The distance between the two adjacent lattice planes is derived from the experimental peak position using Bragg formula. Experimentally, the Bragg law can be utilized by using X-rays of known wavelength (λ_0) and measuring (θ_{hkl}^{exp}), we can determine the interplanar spacing (d_{hkl}^{exp}) of various planes in a crystal.

$$d_{hkl}^{exp} = \frac{\lambda_0}{2 \sin \theta_{hkl}^{exp}} \quad (\text{III.3})$$

The experimental lattice parameter values (a_{hkl}^{exp}) for Cubic systems can be calculated from the following equation using the (hkl) parameters and the interplanar spacing (d_{hkl}^{exp}) [118].

$$d_{hkl}^{exp} = \frac{a_{hkl}^{exp}}{\sqrt{h^2+k^2+l^2}} \quad (III.4)$$

III.1.2 Scanning electron microscopy (SEM)

Scanning Electron Microscopy (SEM) is one of the most effective techniques for observing texture and evaluating the optical quality of the surface of thin films. This method is non-destructive and enables superficial studies with a resolution of a few nanometers a vast depth of field. Its significant benefit is the variety of information given [119]. It provides information on morphology (shape, size, particles arrangement), topography (determination of surface defects, texture), differences in composition, orientation crystalline and the defects presence. This technique can also allow us to determine the thickness of a thin layer, using a representation of the perpendicular section of this thin layer [107].

When an electron hits the atom, a variety of interaction products are evolved. Figure III.4 displays these different products and their usage to obtain various information about the sample. Scattering of the electron from the electrons of the atom leads to the production of backscattered electrons and secondary electrons. The electron may get transferred through the sample if it is thin. Primary electrons with sufficient energy may knock out the electron from the inner shells of the atom, and the excited atom may relax with the release of Auger electrons or X-ray photons. All these interactions convey information about the sample; For example, Auger electrons, expelled electrons and X-rays have energies unique to the element from which they are originating. These distinctive signals provide information about the chemical identity and composition of the sample [48].

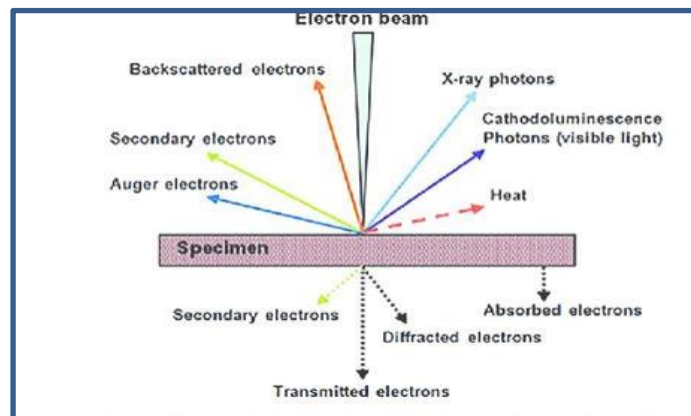


Figure III. 4: variety of interaction products evolved due to interaction of primary electron beam and sample [120].

For the morphological study we used scanning electron microscope (SEM JEOL) model VEGAS3 TESCAN shown in the figure III. 5:



Figure III. 5: Photo of Scanning electron microscope.

III.1.3 UV-Visible spectroscopy

Spectroscopy domains are generally distinguished according to the long interval at which the measurements are taken [98]. The following areas can be distinguished: ultraviolet, visible and infrared. In our case, the technique used was UV- visible spectrophotometry, and by definition, it is an optical method for determining the different optical parameters such as refractive index, extinction coefficient, and the energy gap, transmitted radiation from the detection, absorbed or reflected [120,121]

Ultraviolet-visible spectrophotometer includes the spectroscopy of photons in the ultraviolet range (200–400 nm) and visible range (400–800 nm). It is a type of absorption spectroscopy in which the excitation of the electrons takes place from the ground state to the excited state, whereas fluorescence detects transitions from the excited state to the ground state. The technique is most frequently used quantitatively to estimate concentrations of an absorbing species in the sample using the Beer-Lambert law. The principle involved in UV-VIS Spectroscopy states that when a beam of monochromatic light is passed through a homogeneous medium of an absorbing substance, the rate of decrease in intensity of radiation concerning the thickness of the absorbing medium is directly proportional to the intensity of the incident radiation as well as the concentration of the medium [48,121].

$$I = I_0 \cdot \exp(-\alpha d) \quad (\text{III.5})$$

Where α is the absorption coefficient, d is the thickness of the film, I_0 and I are the intensity of the incident and the transmitted beams, respectively. The absorption coefficient (α) can be calculated using the following expression:

$$\alpha = \frac{1}{d} \ln\left(\frac{100}{T\%}\right) \quad (\text{III.6})$$

Where T (%) is the transmittance (quantity of the transmitted light), and can be directly measured by:

$$T(\%) = \frac{I}{I_0} \times 100 \quad (\text{III.7})$$

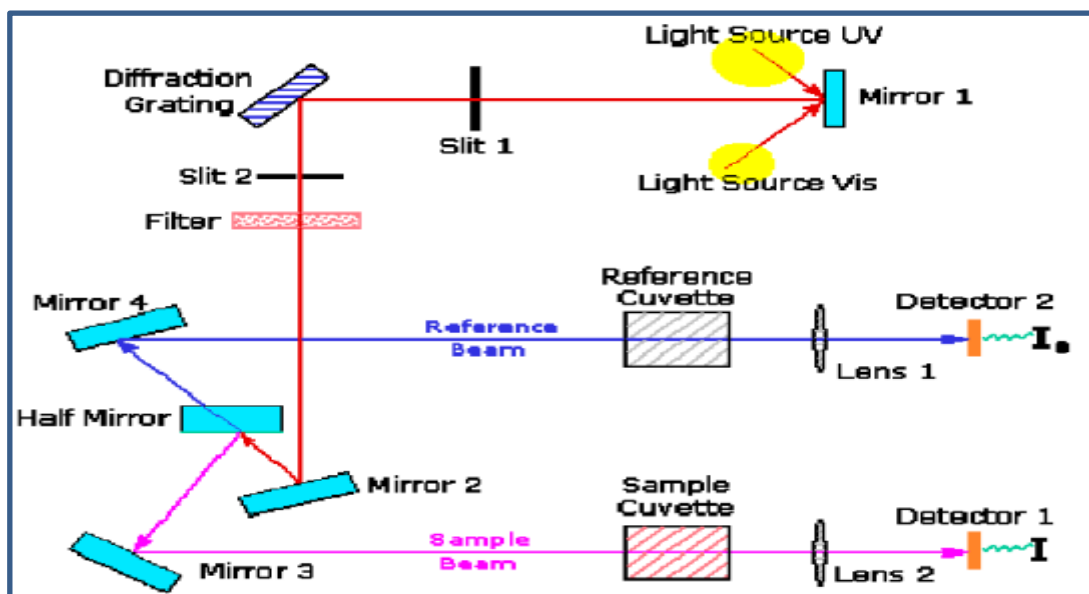


Figure III. 6: Schematic of UV-Visible spectrophotometer [48,122].

For optical transmission spectra we have used an UV-visible spectrophotometer (Shimadzu, Model 1800) as shown in figure III. 7:



Figure III. 7: UV-Visible Spectrophotometer.

III.2 Results and discussion

This section highlights the structural and optical properties by discussing the obtained results revealed using XRD and SEM as structural and morphological techniques and UV-Vis as optical analyses.

III.2.1 Structural study

The determination of the crystalline structure and orientation of our elaborated thin films has been carried out using their XRD spectra, the various peaks that define the structure of pure In_2O_3 and $[\text{SmO}_3; \text{In}_2\text{O}_3]$ thin films are shown in **Figure III. 8** deposited on glass substrates and annealed at 420°C for the deposition time (t) equals 4 min.

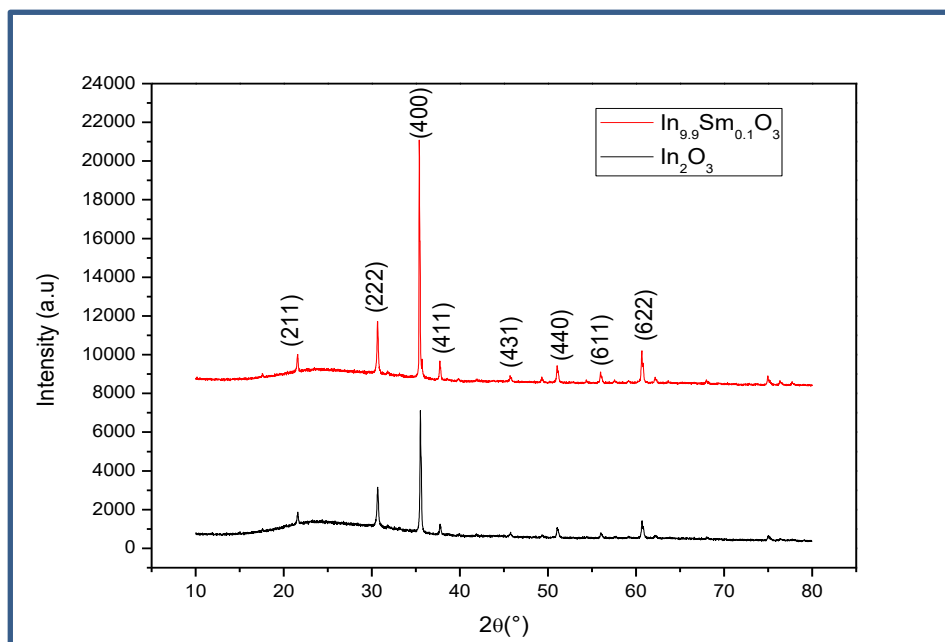


Figure III. 8: XRD patterns of pure In_2O_3 and $[\text{SmO}_3; \text{In}_2\text{O}_3]$.

Figure III. 8 denote the X-ray diffraction patterns of undoped and Sm doped indium oxide thin films. These samples exhibit well defined diffraction peaks located at $2\theta = 21.499^\circ$, $2\theta = 30.581^\circ$, $2\theta = 35.467^\circ$, $2\theta = 37.686^\circ$, $2\theta = 45.692^\circ$, $2\theta = 51.039^\circ$, $2\theta = 55.992^\circ$, $2\theta = 60.678^\circ$ correspondings to reflections of the planes (211), (222), (400), (411), (431), (440), (611), (622), respectively. These peaks belong to a bixbyite cubic structure with a space group of Ia-3 according to [Joint Committee on Powder Diffraction Standards (JCPDS) data card No. 06-0416][123]. The presence of several peaks indicates that the films are polycrystalline [124].

The XRD spectrum of $\text{In}_{0.9}\text{Sm}_{0.1}\text{O}_3$ reveals a preferential orientation peak located at $2\theta = 35.392^\circ$ corresponding to (400) due to its high intensity of 13053 (ua) comparing to the other

peaks. The growth along the (400) plane is due to the low free surface energy found in this direction for the In_2O_3 cubic structure[51]. However, we note the presence of another main peak (222) located at $2\theta = 30.646^\circ$, suggesting that the film is polycrystalline in nature as we mentioned before; by meaning there is a preferential growing competition between (222) and (400) planes, this indicates that doping has an important effect on the growth mechanism of the In_2O_3 films deposited by the pneumatic spray process.

Table III. 1: ASTM file of In_2O_3 .

Date: 21/09/2021 Time: 14:52:41				File: 00-001-0929		
No.	h	k	l	d [Å]	2Theta[deg]	I [%]
1	2	0	0	5,06000	17,513	1,0
2	2	1	1	4,13000	21,499	14,0
3	2	2	2	2,92100	30,581	100,0
4	3	2	1	2,70400	33,103	2,0
5	4	0	0	2,52900	35,467	30,0
6	4	1	1	2,38500	37,686	8,0
7	4	2	0	2,26200	39,819	2,0
8	3	3	2	2,15700	41,846	6,0
9	4	2	2	2,06600	43,782	2,0
10	4	3	1	1,98400	45,692	10,0
11	5	2	1	1,84800	49,269	4,0
12	4	4	0	1,78800	51,039	35,0
13	4	3	3	1,73500	52,716	4,0
14	6	0	0	1,68600	54,372	2,0
15	6	1	1	1,64100	55,992	6,0
16	6	2	0	1,60000	57,559	2,0
17	5	4	1	1,56100	59,137	4,0
18	6	2	2	1,52500	60,678	25,0
19	6	3	1	1,49200	62,167	6,0
20	4	4	4	1,46000	63,687	6,0
21	5	4	3	1,43100	65,135	2,0
22	6	4	0	1,40300	66,602	2,0
23	7	2	1	1,37700	68,029	4,0
24	6	4	2	1,35200	69,465	2,0
25	6	5	1	1,28500	73,662	4,0

a) Lattice parameters

Based on Miller indices and equations (III.3) and (III.4) we calculated the inter-reticular distances d_{hkl} of the most intense peaks in the two iron oxide samples and the cell a parameters respectively

Table III. 2: Shows the inter-planer spacing and lattice parameter a of the undoped and Sm doped In_2O_3 .

	$2\theta(^{\circ})$	Hkl	I(a.u)	$d_{hkl}(\text{\AA})$	a (\AA)
[SmO ₃ ; In ₂ O ₃]	35.392	400	13053	2.533	0.633
	30.646	222	3682	2.913	0.841
In ₂ O ₃	35.509	400	6964	2.529	0.629
	30.646	222	3107	2.921	0.842

b) Crystallites size

The average crystallites size deduced from the full width at half the maximum (FWHM) of (400) and (222) planes using the equation (III.2), and table below shows the crystalline size D of the undoped and Sm doped In_2O_3 thin films.

Table III. 3: Shows the crystalline size D of the undoped and Sm doped In_2O_3 thin films.

	hkl	FWHM ($^{\circ}$)	D_{hkl} (nm)
[SmO ₃ ; In ₂ O ₃]	222	0.1602	52
	400	0.1460	56
[In ₂ O ₃]	222	0.1828	45
	400	0.1809	45

III.2.2 Surface and morphological study

The surface morphology of films depends on the deposition technique and its parameters, and it may influence the films' mechanical, electrical, and optical properties. Figure III.9 shows the scanning electron micrographs of undoped (Figure III.9(a)) and Sm doped indium oxide (Figure III.9(b)) thin films. The images indicate that the film's surface morphologies are void-free and exhibit a densely packed structure with uniform particle size. It is observed that the surface morphology of the films varies with doping, leading to changes in the film thickness. The films are formed with a dense granular structure with regular grains. The grain size on top of the film increases with doping; as a result, increasing in thickness (figure III.9 (b)).

It is clear that this thin film exhibits a dense inner structure without any pinholes and cracks, indicating that the film is rough, well adherent to the substrate and the surface is granular and compact. In addition, this micrograph shows that grains with pyramidal shapes are formed indicate that the film is rough.

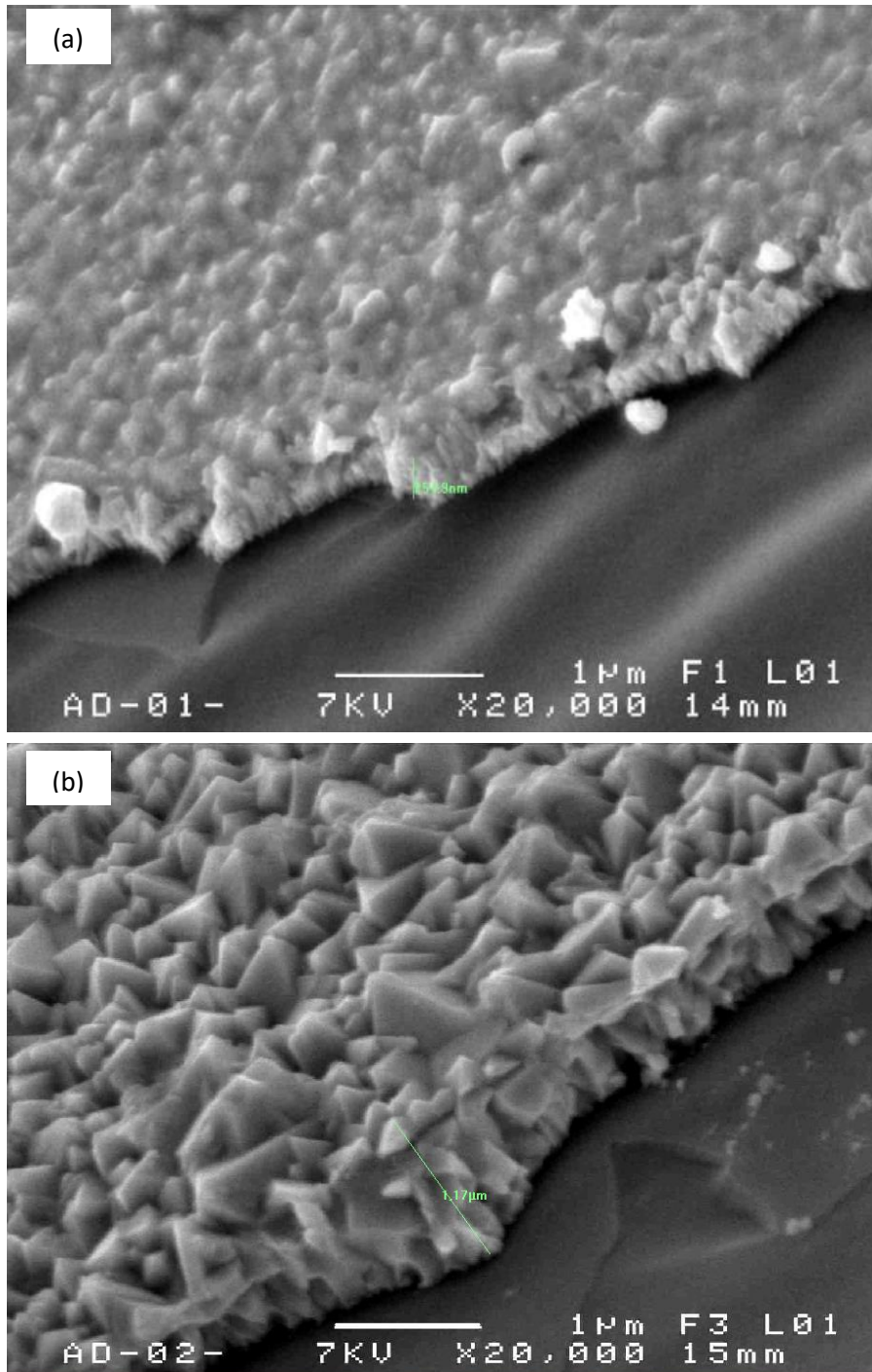


Figure III. 9: SEM surface images of: a) pure In_2O_3 b) $\text{In}_{0.9}\text{Sm}_{0.1}\text{O}_3$ thin films.

III.2.3 Optical study

The optical transmittance measured as a function of the wavelength is depicted in Figure III. 10:

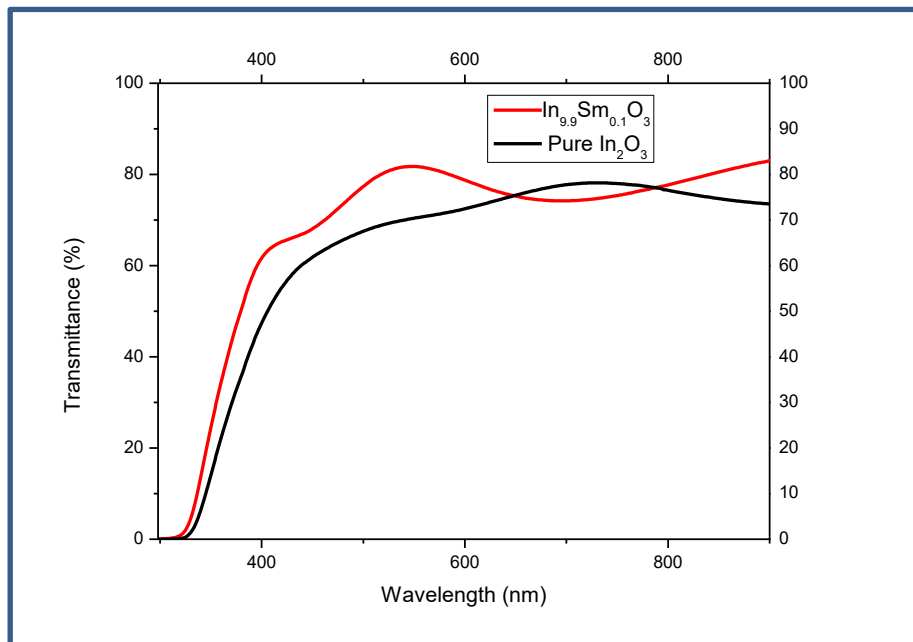


Figure III. 10: Optical transmittance spectra of In_2O_3 thin films as a function of the wavelength.

Figure III. 10 shows the optical transmittance measured as a function of the wavelength. the undoped and Sm doped In_2O_3 thin films exhibit identical transmittance in the wavelength range [400-900nm], even though the transmittance of Sm doped In_2O_3 is higher than the pure indium oxide undoped and Sm doped In_2O_3 ; which means, $[\text{SmO}_3; \text{In}_2\text{O}_3]$ is thicker than the pure indium oxide. This is due to the layers high crystalline quality.

The abrupt drop in transmission for wavelengths less than 400 nm corresponds to the threshold of the absorption energy of the In_2O_3 film due to the transition between the valence band and the conduction band. Note that the transmittance in our case does not have the same behaviour for undoped and sm doped indium oxide.

Figure III. 10 illustrates a transmittance-wavelength spectrum obtained by optical spectroscopy. all layers show a good optical transparency. we can observe that these films have a high transmittance (>75%) in visible regions and high absorption (near 80%) in ultraviolet regions. The curves showed that the transmittance of thin layers decreases after doping. This decrease in the transmittance of thin films can be due to doping, which increases the thickness of the thin layers and increases the surface roughness, leading to more optical scattering.

As the increases, the average transmittance of the films reduces slightly. It would be noted that the film at a higher thickness becomes nearly opaque to the near-infrared region. This is due to the high carrier concentration, which absorbs photons.

- **Optical bandgap**

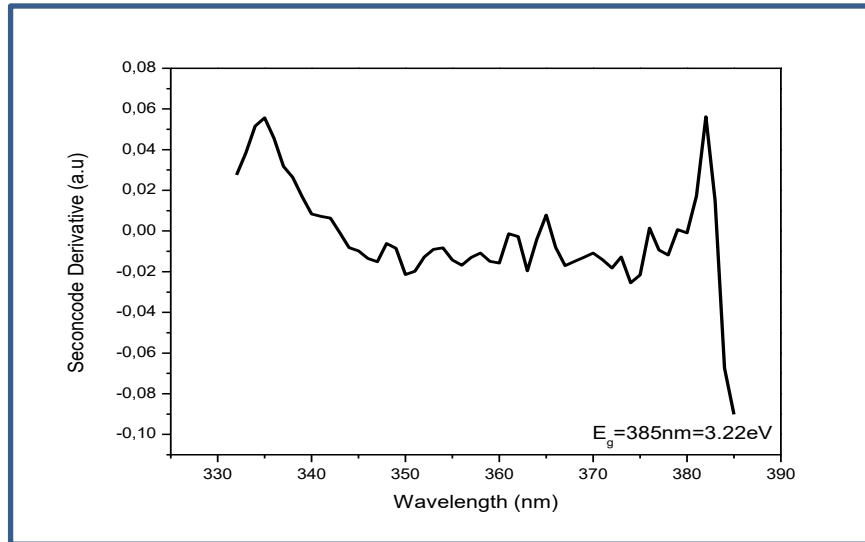


Figure III. 11: Optical band gap spectra of pure indium oxide In_2O_3 .

The Figure III. 11 represents the optical band gap spectra of pure indium oxide In_2O_3 , the gap is equal to 3.22 eV, this value is determined using the second derivative method.

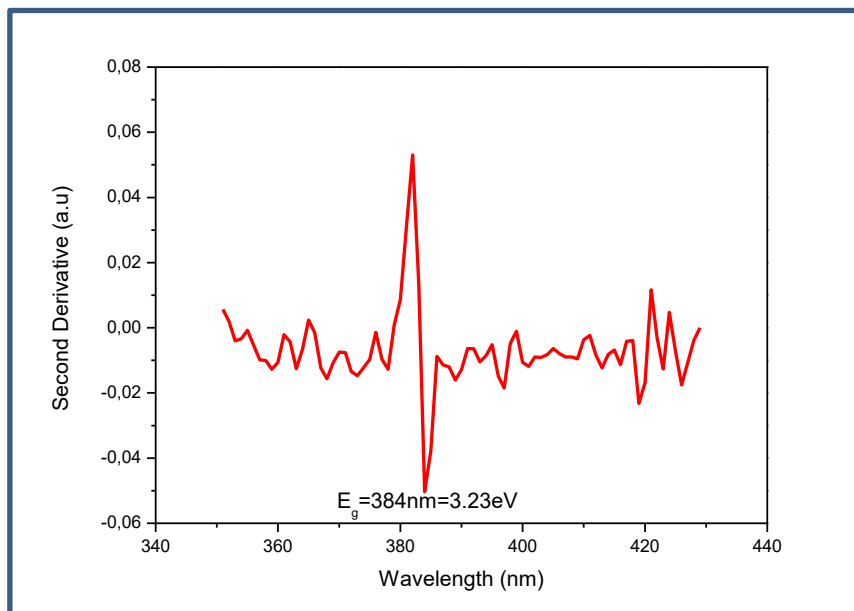


Figure III. 12: optical band gap spectra of Sm doped Indium Oxide [SmO_3 ; In_2O_3].

The Figure III. 12 represents the optical band gap spectra of Sm doped indium oxide In_2O_3 , the gap is equal to 3.23 eV, this value is determined using the second derivative method.

Sm doped indium oxide [$\text{SmO}_3; \text{In}_2\text{O}_3$] exhibits larger band gap 3.23 eV (Figure III. 11) than the pure In_2O_3 (figure III. 12); this is due to the decrease of disorder in the film network, this decreasing is because of the increase in crystalline quality. On the other hand, the oxygen concentration in pure and Sm doped indium oxide plays a significant role in increasing optical band gap, this means doping with samarium oxide causes the increase of oxygen vacancies. The latter causes augment in the optical band gap due to carrier concentration in the [$\text{SmO}_3; \text{In}_2\text{O}_3$] thin films.

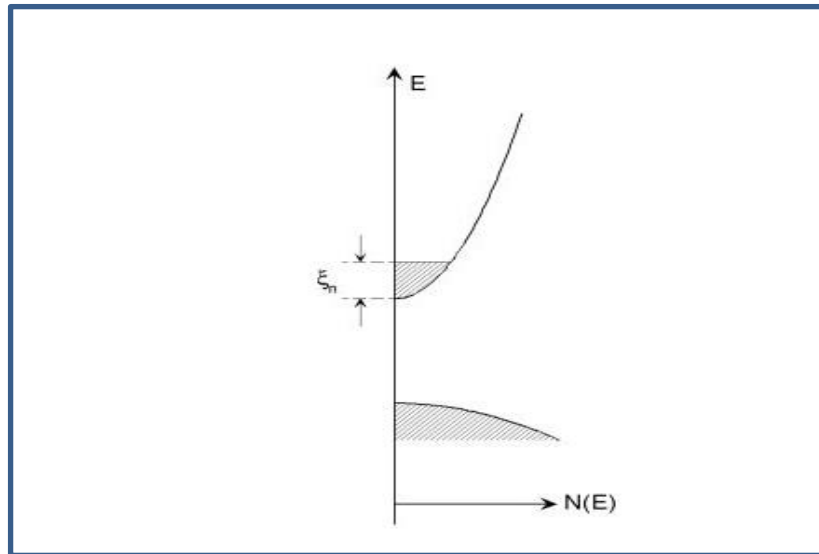


Figure III. 13: Energy versus density of states diagram for n- type degenerate semiconductor.

If the semiconductor is heavily doped, the Fermi level is in the band (conduction band for n-type material, valence band for p-type material) by a quantity of ξ . This is shown in the Figure III. 13 for an n-type material. Since the states below ξ_n are already filled, fundamental transitions to states below $E_g + n \xi$ are forbidden. Therefore, the absorption edge should shift to higher energies by about ξ_n the shift of the absorption edge due to band filling is known as the Burstein-Moss shift.

General Conclusion

General conclusion

Undoped and doped In_2O_3 thin films have been successfully prepared using pneumatic spray pyrolysis. The films have been deposited on glass substrates. The structural properties of the deposited films have been analyzed using X-ray diffraction (XRD), and the optical properties have been analyzed by UV-VIS spectroscopy, while the morphological properties were extracted using scanning electron microscopy.

The experimental results and the characterization of undoped and doped indium oxide films are explained in the third part of the thesis presenting the structural, morphological, and optical properties.

Either a reduction in the oxygen content in the film or an increase in the film thickness The films have a rough surface, and the morphology of the grains varies as the preferred growth direction changes, producing grains with a pyramidal shape.

The XRD results prove that the obtained films exhibit a cubic polycrystalline nature with a variety of orientations. Preferential growth orientation a (400) plane.

SEM images show that the films have a rough surface, and the morphology of the grains varies as the preferred growth direction changes, producing grains with a pyramidal shape.

Optical characterization revealed that our films are transparent, with a 75% to 80% transparency range. Furthermore, the improvement in transmittance of thin films was related to the films' crystalline quality, surface roughness, and oxygen content in the film. We also discovered that the optical gap varied between 3.22 and 3.23 eV.

Finally, there is an essential factor in achieving the optimal attributes after doping, which directly impacts structural, optical, and morphological properties. In conclusion, we can suggest that further research is required to improve the performance of this promising material and improve the properties of indium samarium oxide (ISO) thin films, which can be more suitable for many applications such as optoelectronic photovoltaic, etc.

References

- [1] R. J. Deokate, "Influence of Spray Solution Quantity on Microstructural and Optical Properties of In₂O₃ Thin Films Prepared by Spray Pyrolysis", *Macromol. Symp*, 2020.
- [2] A. Nakane et al, "Transparent conductive oxides", Springer Ser. Opt. Sci, 2018.
- [3] S. Ahmmed, A. Aktar, F. Rahman, and J. Hossain, "Optik A numerical simulation of high efficiency CdS / CdTe based solar cell using NiO HTL and ZnO TCO", *Optik*, 2020.
- [4] R. A. Afre, N. Sharma, M. Sharon, and M. Sharon, "Transparent conducting oxide films for various applications: A review", *Rev. Adv. Mater. Sci*, 2018.
- [5] D. S. Ginley, C. Bright, and G. Editors, "Transparent Conducting Oxides", 2000,.
- [6] B. G. Lewis and D. C. Paine, "Applications and Processing of Transparent Conducting Oxides", 2000.
- [7] G. Hosamani, B. N. Jagadale, J. Manjanna, S. M. Shivaprasad, D. K. Shukla, and J. S. Bhat, "Structural, Optical and Magnetic Properties of Dy-doped In₂O₃ Nanoparticles ", *J. Electron. Mater*, 2021.
- [8] J. Joseph Prince, S. Ramamurthy, B. Subramanian, C. Sanjeeviraja, and M. Jayachandran, "Spray pyrolysis growth and material properties of In₂O₃ films", *J. Cryst. Growth*, 2002.
- [9] S. Kaleemulla, A. S. Reddy, S. Uthanna, and P. S. Reddy, "Physical properties of In₂O₃ thin films prepared at various oxygen partial pressures", *J. Alloys Compd*, 2009.
- [10] V. Reymond, "thesis de doctorat," 2004.
- [11] A. Mosbah, "Elaboration Et Caracterisation De Couches Minces D'Oxyde De Zinc, These doctorat", *Université Mentouri Constantine*, 2009.
- [12] N. Bouhssira, "Elaboration et Caractérisation des Couches Minces d'Oxyde de Zinc par Evaporation, Magister". *Université Mentouri Constantine*, 2005.
- [13] J. A. Venables, "Atomic processes in crystal growth", *Surf. Sci*, 1994.
- [14] K. Oura, M. Katayama, A. V. Zotov, V. G. Lifshits, and A. A. Saranin, "Growth of Thin Films", 2003.
- [15] K. Reichelt, "Nucleation and growth of thin films", 1988.
- [16] A. Rockett, "The Materials Science of Semiconductors", Springer, Boston, MA, 2008.
- [17] J. A. Venables, G. D. T. Spiller, and M. Hanbucken, "Nucleation and growth of thin films", *Reports Prog. Phys* 1984.
- [18] J. A. Venables, "Nucleation growth and pattern formation in heteroepitaxy", *Phys. A Stat. Mech. its Appl*, 1997.
- [19] E. Bauer and J. H. van der Merwe, "crystalline superlattices: From", *Phys. Rev. B*, 1986.
- [20] S. Stoyanov and I. Markov, "On the 2D-3D transition in epitaxial thin film growth", *Surf. Sci*, 1982.
- [21] A. Marty and S. Andrieu, "Croissance et structure des couches minces", *J. Phys. IV* 1996.
- [22] M. Heuberger, G. Dietler, and L. Schlapbach, "New aspects in Volmer-Weber 3D growth: an XPS intensity study applied to thin films of Au and Ce on polypropylene", *Surf. Sci*, 1994.
- [23] C. Ratsch and J. A. Venables, "Nucleation theory and the early stages of thin film growth", *J. Vac. Sci. Technol. A Vacuum, Surfaces, Film*, 2003.
- [24] F. Yanineb, "Contribution à l'élaboration de couches minces d'Oxydes Transparents Conducteurs (TCO)", *Université Mentouri Constantine*, 2010.
- [25] J. E. Greene, "Thin Film Nucleation, Growth, and Microstructural Evolution: An Atomic",

- Scale View, Third Edit. Elsevier Ltd., 2010.
- [26] M. Anitha, K. Saravanakumar, N. Anitha, I. Kulandaisamy, and L. Amalraj, "Materials Science & Engineering B Influence of annealing temperature on physical properties of Sn-doped CdO thin films by nebulized spray pyrolysis technique", *Mater. Sci. Eng. B*, 2019.
- [27] G. J. Exarhos and X. D. Zhou, "Discovery-based design of transparent conducting oxide films", *Thin Solid Films*, 2007.
- [28] S. Calnan and A. N. Tiwari, "High mobility transparent conducting oxides for thin film solar cells", *Thin Solid Films*, 2010.
- [29] H. Liu, V. Avrutin, N. Izyumskaya, Ü. Özgr, and H. Morkoç, "Transparent conducting oxides for electrode applications in light emitting and absorbing devices", *Superlattices and Microstructures*, 2010.
- [30] P. D. C. King and T. D. Veal, "Conductivity in transparent oxide semiconductors" *Journal of Physics Condensed Matter*, 2011.
- [31] M. R. R. Waugh, "The synthesis, characterisation and application of transparent conducting thin films", doctorate thesis, University of college London, 2011.
- [32] S. Shirakata, T. Sakemi, K. Awai, and T. Yamamoto, "Electrical and optical properties of large area Ga-doped ZnO thin films prepared by reactive plasma deposition", *Superlattices Microstruct.*, 2006.
- [33] S. C. Dixon, D. O. Scanlon, C. J. Carmalt, and I. P. Parkin, "N-Type doped transparent conducting binary oxides: An overview", *J. Mater. Chem. C*, 2016.
- [34] A. Höpe, "Diffuse Reflectance and Transmittance", 2014.
- [35] T. J. Coutts, D. L. Young, and X. Li, "Characterization of transparent conducting oxides", *MRS Bull*, 2000.
- [36] T. S. Moss, "The interpretation of the properties of indium antimonide", *Proc. Phys. Soc. Sect. B*, 1954.
- [37] G. Haacke, "New figure of merit for transparent conductors", *J. Appl. Phys*, 1976.
- [38] C. Schaefer, G. Bräuer, and J. Szczyrbowski, "Low emissivity coatings on architectural glass", *Surf. Coatings Technol*, 1997.
- [39] E. A. Forsh et al, "Optical and photoelectrical properties of nanocrystalline indium oxide with small grains", *Thin Solid Films*, 2015.
- [40] A. Raza, O. . Agnihotri, and B. . Gupta, "Preparation and intrinsic absorption in the band edge in chemically sprayed In , O , layers", 1977.
- [41] M. Girtan and G. Folcher, "Structural and optical properties of indium oxide thin films prepared by an ultrasonic spray CVD process", 2003.
- [42] A. Moses Ezhil Raj et al, "Growth mechanism and optoelectronic properties of nanocrystalline In₂O₃ films prepared by chemical spray pyrolysis of metal-organic precursor", *Phys. B Condens. Matter*, 2008.
- [43] R. L. Weiher and R. P. Ley, "Optical properties of indium oxide", *J. Appl. Phys*, 1966.
- [44] G. B. González, J. S. Okasinski, T. O. Mason, T. Buslaps, and V. Honkimäki, "In situ studies on the kinetics of formation and crystal structure of In₄ Sn₃ O₁₂ using high-energy x-ray diffraction", *J. Appl. Phys*, 2008.
- [45] H. Kim et al, "Electrical, optical, and structural properties of indium-tin-oxide thin films for organic light-emitting devices", *J. Appl. Phys* 1999.
- [46] L. Dai, X. L. Chen, J. K. Jian, M. He, T. Zhou, and B. Q. Hu, "Fabrication and characterization of In₂O₃ nanowires", *Appl. Phys. A Mater. Sci. Process*. 2002.

- [47] V. V. Pillay, "Structural, Optical and Electrecal characterization of indium oxide and aluminum nitride thin films for gas sensing application", Research Department of Physics Bishop Heber College, 2012.
- [48] Y. Anouar, "Optimization of indium oxide thin films properties prepared by sol gel spin coating process for optoelectronic application", doctorate thesis, university of Biskra, 2020.
- [49] E. Savarimuthu et al, "Synthesis and materials properties of transparent conducting In₂O₃ films prepared by sol-gel-spin coating technique", J. Phys. Chem. Solids, 2007.
- [50] I. Elfallal, R. D. Pilkington, and A. E. Hill, "Formulation of a statistical thermodynamic model for the electron concentration in heavily doped metal oxide semiconductors applied to the tin-doped indium oxide system", Thin Solid Films, 1993.
- [51] A. Bouhdjer et al, "Influence of annealing temperature on In₂O₃ properties grown by an ultrasonic spray CVD process", Optik (Stuttg), 2016.
- [52] Y. Liu, W. Xu, D. B. Liu, M. Yu, Y. H. Lin, and C. W. Nan, "Enhanced thermoelectric properties of Ga-doped In₂O₃ ceramics via synergistic band gap engineering and phonon suppression", Phys. Chem, 2015.
- [53] O. Warschkow, D. E. Ellis, G. B. González, and T. O. Mason, "Defect Structures of Tin-Doped Indium Oxide", J. Am. Ceram. Soc, 2003
- [54] M. Marezio, "Refinement of the crystal structure of In₂O₃ at two wavelengths", 1966
- [55] F. HADJERSI, "Investigation des propriétés structurales, optiques et électriques des films ITO élaborés par pulvérisation cathodique RF; Effet du recuit", 2011.
- [56] K. Daoudi, "ELElaboration et caractersation de films minces d'Oxyde D'indium dope a l'etain obtenue par voie SOL-GEL potentialité pour la réalisation d'electrodes sur silicium poreux", Kais Daoudi, 2006.
- [57] M. Epifani, P. Siciliano, A. Gurlo, N. Barsan, and U. Weimar, "Ambient Pressure Synthesis of Corundum-Type In₂O₃", J. Am. Chem. Soc, 2004.
- [58] O. Bierwagen, "Indium oxide - A transparent, wide-band gap semiconductor for (opto)electronic applications", Semicond. Sci. Technol, 2015.
- [59] J. J. Prince, S. Ramamurthy, B. Subramanian, and C. Sanjeeviraja, "Spray pyrolysis growth and material properties of In₂O₃ films", 2002.
- [60] O. N. Mryasov and A. J. Freeman, "Electronic band structure of indium tin oxide and criteria for transparent conducting behavior", Phys. Rev. B - Condens. Matter Mater, 2001
- [61] J. Stankiewicz, X. Torrelles, J. L. García-Muñoz, and J. Blasco, "Structural and electrical properties of indium oxide thin films grown by pulsed laser deposition in oxygen ambient", J. Alloys Compd, 2017.
- [62] M. Anwar, I. M. Ghauri, and S. A. Siddiqi, "The study of optical properties of In₂O₃ and of mixed oxides In₂O₃-MoO₃ system deposited by coevaporation", J. Mater. Sci., 2006.
- [63] A. A. Dakhel, "Effect of ytterbium doping on the optical and electrical properties of intrinsic In₂O₃ thin films", Microelectron. Reliab, 2010.
- [64] H. K. Müller, "Electrical and Optical Properties of Sputtered In₂O₃ films. I. Electrical Properties and Intrinsic Absorption", Phys. Status Solidi, 1968.
- [65] A. Attaf, A. Bouhdjer, H. Saidi, M. S. Aida, N. Attaf, and H. Ezzaouia, "On tuning the preferential crystalline orientation of spray pyrolysis deposited indium oxide thin films", Thin Solid Films, 2017.
- [66] A. Bouhdjer, "Study of Thin Layers of Indium Oxide (In₂O₃) Elaborated by Chemical Means", 2016.

- [67] K. K. Makhija, A. Ray, R. M. Patel, U. B. Trivedi, and H. N. Kapse, "Indium oxide thin film based ammonia gas and ethanol vapour sensor," *Bull. Mater. Sci*, 2005.
- [68] C. M. Ghimbeu, "Préparation et Caractérisation de couches minces d'oxydes métalliques semiconducteurs pour la détection de gaz polluants atmosphériques' Thèses Doctorat", Université Paul Verlaine de Metz, 2007.
- [69] M. GHOUGALI, "Elaboration and characterization of nanostructuring NiO thin films for gas sensing applications", doctorat thesis, 2019.
- [70] H. Sainthiya and N. S. Beniwal, "Different types of cooling systems used in photovoltaic module solar system: A review", 2018.
- [71] A. El Hichou et al, "Effect of substrate temperature on electrical, structural, optical and cathodoluminescent properties of In₂O₃-Sn thin films prepared by spray pyrolysis", *Thin Solid Films*, 2004.
- [72] J. M. Klinger, "A historical geography of rare earth elements: From discovery to the atomic age", *Extr. Ind. Soc*, 2015.
- [73] J.H.L.Voncken, "The Rare-Earth Elements: An introduction", 2016.
- [74] J. H. L. Voncken, "Physical and Chemical Properties of the Rare Earths", 2016.
- [75] N. Nakamura, H. Nakagawa, K. Koshida, and M. Niiya, "Proceeding of the 5th International Display workshops", 1998.
- [76] D. O. Meyer, "Sputtering by particle bombardment I: Physical sputtering of single-elements solids", 1982.
- [77] K. Wasa, I. Kanno, and H. Kotera, "Sputter Deposition Technology: Fundamentals and Applications for functional Thin films", 2nd ed, William Andrew publishing, 2012.
- [78] N. Abdelouahab, "Preparation and characterization of thin films nanostructures based on ZnO and other oxides" phd thesis.
- [79] T. Motohiro, "Computer Simulation," 2012.
- [80] M. Henini, "Molecular beam epitaxy", *Mol. Beam Ep*, 2013.
- [81] S. Franchi, "Molecular beam epitaxy: fundamentals, historical background and future prospects", Elsevier Inc, 2013.
- [82] D. V. M. and K. Boar, "An introduction to semiconductor technology", 2nd editio. John Wiley & sons, 1920.
- [83] M. C. RAO, "Pulsed Laser Deposition — Ablation Mechanism and Applications", *Int. J. Mod. Phys. Conf. Ser*, 2013.
- [84] Z. Liu, "Laser Applied Coatings", 2010.
- [85] S. R. V. Siva Prasanna, K. Balaji, S. Pandey, and S. Rana, "Metal Oxide Based Nanomaterials and Their Polymer Nanocomposites". Elsevier Inc, 2018.
- [86] O. Nur and M. Willander, "Conventional nanofabrication methods", 2020.
- [87] M. Bellardita, A. Di Paola, S. Yurdakal, and L. Palmisano, "Preparation of catalysts and photocatalysts used for similar processe in Heterogeneous Photocatalysis: Relationships with Heterogeneous Catalysis and Perspectives", Elsevier B.V, 2019.
- [88] A. M. Whelan, "Sol-Gel Sensors", 2017.
- [89] J. Livage and C. Sanchez, "Sol-gel chemistry", *J. Non. Cryst. Solids*, 1992.
- [90] C. . Brinker, A. . Hurd, and G. C. Frye, "SOL-GEL thin film Formation", 1990.
- [91] A. E. Amrani, "Thèse de doctorat", Université de Limoges, 2008.
- [92] G. Srinivasan, N. Gopalakrishnan, Y. S. Yu, R. Kesavamoorthy, and J. Kumar, "Influence of post-deposition annealing on the structural and optical properties of ZnO thin films prepared by sol-gel and spin-coating method", *Superlattices Microstruct*, 2008.
- [93] L. L. Hench and D. R. Ulrich, "Ultrastructure Processing of Ceramics, Glasses, and Composites", Wiley-Interscience, 1984.

- [94] J. B. Mooney and S. B. Radding, "Spray Pyrolysis Processing", *Annu. Rev. Mater. Sci.*, 1982.
- [95] S. M. Sabnis, "Process flow of spray pyrolysis technique", *IOSR J. Appl. Phys.*, 2013.
- [96] M. Khammar, "Etude d'un jet en spray d'une solution chimique sur un substrat chaud destiné à l'élaboration des couches minces", university of Mentouri Constantine, 2010.
- [97] T. V. Gavrilović, D. J. Jovanović, and M. D. Dramićanin, "Synthesis of multifunctional inorganic materials: From micrometer to nanometer dimensions", *Nanomater. Green Energy*, 2018.
- [98] O. MOHAMED, "Synthesis and characterization of Zinc Oxide (ZnO) Thin films deposited by spray pyrolysis for applying: electronics and photonics. phd thesis", University of Biskra, 2018.
- [99] D. Dobkin and M. K. Zuraw, "Principles of chemical vapor deposition", Kluwer Academic Publishers & Springer Science, 2003.
- [100] K. L. Chopra. and E. McGraw, "Thin films phenomena", Hill Co. London, 1975.
- [101] O. Mohamed, "Dépôt et caractérisation des couches minces d'oxyde de Zinc par spray pyrolyse Ultrasonique", magister thesis, Université de Biskra, 2010.
- [102] B. Rogier, "Couches minces de zircone sur polymères: propriétés adhésives et interfaciales", doctorate thesis, univ Haute Alsace, Mulhouse, 1998.
- [103] P. S. Patil, "Versatility of chemical spray pyrolysis technique", *Mater. Chem. Phys.*, 1999.
- [104] W. kern M.T Duffy, "Chemical vapor deposition of aluminum oxides films from organo-aluminum compounds", 1970.
- [105] R. Ayouchi, F. Martin, D. Leinen, and J. R. Ramos-Barrado, "Growth of pure ZnO thin films prepared by chemical spray pyrolysis on silicon", *J. Cryst. Growth*, 2003.
- [106] R. Ayouchi, D. Leinen, F. Martín, M. Gabas, E. Dalchiele, and J. R. Ramos-Barrado, "Preparation and characterization of transparent ZnO thin films obtained by spray pyrolysis", *Thin Solid Films*, 2003
- [107] C. M. Ghimbeu, "Préparation et Caractérisation de couches minces d'oxydes métalliques semiconducteurs pour la détection de gaz polluants atmosphériques", doctorat thesis, l'Université Paul Verlaine de Metz, 2007.
- [108] D. Perednis and L. J. Gauckler, "Thin film deposition using spray pyrolysis", *J. Electroceramics*, 2005.
- [109] M. B. Tahir, M. Rafique, M. S. Rafique, T. Nawaz, M. Rizwan, and M. Tanveer, "Photocatalytic nanomaterials for degradation of organic pollutants and heavy metals". Elsevier Inc, 2020.
- [110] J. Leng, Z. Wang, and J. Wang, *Advances in nanostructures fabricated via spray pyrolysis and their applications in energy storage and conversion. Chemical Society Reviews*, 2019.
- [111] S. Major, A. Banerjee, and K. L. Chopra, "Highly transparent and conducting indium-doped zinc oxide films by spray pyrolysis," *Thin Solid Films*, 1983.
- [112] G. . Wehner, *Phys.Rev.* 1971.
- [113] G. Blandenet, M. Court, and Y. Lagarde, "Thin layers deposited by the pyrosol process," *Thin Solid Films*, 1981.
- [114] G. E. Patil, D. D. Kajale, V. B. Gaikwad, and G. H. Jain, "Spray Pyrolysis Deposition of Nanostructured Tin Oxide Thin Films", 2012.
- [115] S. H. Ng, J. Wang, D. Wexler, S. Y. Chew, and H. K. Liu, 2007.
- [116] M. Thomson, "The Modification of Thin Film Surface Structure via Low Temperature Atmospheric Pressure CVD Post Process Treatment Material", Doctoral Thesis, 2013.
- [117] Saravanakannan and T. Radhakrishnan, "Structural, electrical and optical characteri_zation of CuO thin films prepared by spray pyrolysis technique", *Int. J. ChemTech Res.*, 2014.
- [118] L. Cattin, B. A. Reguig, A. Khelil, M. Morsli, K. Benchouk, and J. C. Berne`de, "Proper_ties of NiO thin films deposited by chemical spray pyrolysis using different precursor solutions", *Appl. Surf. Sci.*, 2008.

- [119] F. Bouaich, "Dopage et caractérisation des couches minces d'oxyde de Zinc déposée par Spray Pyrolyse Ultrasonique", mémoire de magister, Université de Biskra, 2010.
- [120] S. Yilmaz and H. B. Ozmen, "High performance concrete technology and applications", 2016.
- [121] S.Hallynck, "Elaboration et caractérisation de composites chargés en ferrite spinelle à morphologie contrôlée pour utilisation micro-ondes" , phd thesis strasbourg I- louis pasteur, 2005.
- [122] S. Sheth, "Synthesis and Characterization of Catalysts for Photo-oxidation of Water", PhD Thesis, University of Paris-Sud, 2013.
- [123] A. Umar, B. Karunagaran, E. K. Suh, and Y. B. Hahn, "Structural and optical properties of single-crystalline ZnO nanorods grown on silicon by thermal evaporation", Nanotechnology, 2006.
- [124] T. V. Vimalkumar, N. Poornima, C. S. Kartha, and K. P. Vijayakumar, "Effect of precursor medium on structural, electrical and optical properties of sprayed polycrystalline ZnO thin films", Mater. Sci. Eng. B Solid-State Mater. Adv. Technol, 2010.

Abstract

Our work concerns the elaboration and the characterization of the conducting transparent oxide thin films of undoped and samarium doped indium oxide. The pneumatic spray pyrolysis technique has grown these films using indium chloride as precursor solution (InCl_3).

In the first part of this thesis, we realized pure indium oxide [In_2O_3] and the samarium doped indium oxide using the mixture [$\text{SmO}_3: \text{In}_2\text{O}_3$]. We studied the structural, morphological, and optical properties of these thin films. Various characterization techniques of materials analyze these films. The structural characterization of films by analysis of the X-ray diffraction spectra showed that the films undoped and samarium doped indium oxide present a preferential direction according to the plan (400). The UV-Visible spectrophotometer of these films confirms that it is possible to obtain good transparent films of TCO with a transmittance of about 75 to 85% in the visible range; moreover, there is an increase in the optical bandgap from 3.22 to 3.23 eV.

Based on SEM images, thin films were found to be polycrystalline with a cubic structure. The films are characterized by their rough surface, and the morphology of the grains present a preferred growth direction in a pyramidal shape.

Key words: TCO, Thin films, indium oxide, SmCl_3 , DRX, SEM, Band gap.

Résumé:

Notre travail porte sur l'élaboration et la caractérisation des couches minces des oxydes conducteurs transparents (TCO) de oxyde d'indium pur [In_2O_3] et oxyde d'indium dopé avec samarium [$\text{SmO}_3: \text{In}_2\text{O}_3$]. par la technique spray pneumatic en utilisant chlorure d'indium comme solution de précurseur (InCl_3).

Dans la première partie de cette thèse, nous avons réalisé, oxyde d'indium pur et oxyde d'indium dopé avec samarium en utilisant le mélanges [$\text{SmO}_3: \text{In}_2\text{O}_3$] nous avons étudié les propriétés structural, morphologie et optique.

Ces couches sont analysées par diverses techniques de caractérisation des matériaux. La caractérisation structurale des films par analyse des spectres de diffraction des RX a montré que les films [In_2O_3] et [$\text{SmO}_3: \text{In}_2\text{O}_3$] présentent une direction préférentielle suivant le plan (400). Le spectrophotomètre UV-Visible de ces films confirme qu'il est possible d'obtenir de bons films transparents de TCO avec une transmittance de l'ordre de 75 à 85% dans le visible ; en outre , il y a une augmentation de la bande interdite de 3.22 à 3.23 eV.

basé sur les images de SEM, les couches minces étaient polycristallines avec une structure cubique. Les films sont caractérisés par leur surface rugueuse et la morphologie des grains présente une direction de croissance préférée dans une forme pyramidale.

Mots clés: TCO, Couches minces, d'oxyde d'indium, DRX, MEB, Band interdite

ملخص

ويركز عملنا على تطوير وتوصيف طبقات رقيقة من الأكاسيد الشفافة الموصلة لأكسيد الانديوم النقي [In_2O_3] وأكسيد الانديوم المطعم بالساماريوم باستخدام الخليط [$\text{SmO}_3: \text{In}_2\text{O}_3$] بواسطة تقنية الرش الرئوي باستخدام كلوريد الانديوم كمحلول مصدر (InCl_3). في الجزء الأول من هذه الأطروحة ، أنجزنا أكسيد الانديوم النقي وأكسيد الانديوم المطعم بالساماريوم باستخدام مخاليط [$\text{SmO}_3: \text{In}_2\text{O}_3$] مع دراسة الخصائص البنيوية والمورفولوجية والبصرية.

ويتم تحليل هذه الطبقات من خلال تقنيات مختلفة لتحديد خصائص المواد. أظهر الوصف البنيوي للأفلام بواسطة تحليل انعراج أشعة X أن الأفلام [In_2O_3] و [$\text{SmO}_3: \text{In}_2\text{O}_3$] تظهر اتجاه البلوري المفضل لنمو الحبيبات وفقاً للاتجاه البلوري (400) ويؤكد مقياس الأشعة فوق البنفسجية المرئية لهذه الأفلام أنه من الممكن الحصول على أفلام شفافة جيدة من TCO مع نفاذية تتغير من 75 إلى 85% في الأفلام المرئية ؛ وعلاوة على ذلك ، هناك زيادة في فجوة النطاق المحظور من 3.22 إلى 3.23 إلكترون فولت .

تظهر صور المجهر الإلكتروني الماسح أن الشرائح الرقيقة متعددة التبلور كما انها تتميز لسطحها الخام، كما أن مورفولوجيا الحبيبات تتميز بإجاه نمو مفضل متخذة الشكل الهرمي .

الكلمات المفتاحية: TCO، الشرائح الرقيقة، أكسيد الانديوم، انعراج أشعة X، المجهر الإلكتروني الماسح، النطاق المحظور.